RSC Advances

PAPER

View Article Online
View Journal | View Issue

Cite this: *RSC Adv.*, 2023, **13**, 17074

Design, synthesis, and biological evaluation with molecular dynamics study of novel pyrazolo[3,4-*d*] pyrimidine derivatives as anti-cancer agents†

Rania M. Shaban, [a] Nermin Samir,[b] Yassin M. Nissan[ac] and Khaled A. M. Abouzid *[b]

Received 20th January 2023
Accepted 30th May 2023

DOI: 10.1039/d3ra00446e

rsc.li/rsc-advances

In continuation of our efforts to discover new structural chemotypes with significant chemotherapeutic activities, a novel series of pyrazolo[3,4-*d*]pyrimidine-based compounds linked to a piperazine ring, bearing different aromatic moieties, through different linkages was designed and synthesized as FLT3 inhibitors. All of the newly synthesized compounds were evaluated for their cytotoxicity on 60-NCI cell lines. Compounds with the piperazine acetamide linkage **XIIa–f** & **XVI** exhibited a remarkable anticancer activity among all of the tested compounds, especially against non-small cell lung cancer, melanoma, leukemia and renal cancer models. Furthermore, compound **XVI** (NSC no – 833644) was further screened with a 5-dose assay on nine subpanels and exhibited a GI_{50} between 1.17 and 18.40 μM. On the other hand, molecular docking and dynamics studies were performed to predict the binding mode of the newly synthesized compounds in the FLT3 binding domain. Finally, through a predictive kinetic study, several ADME descriptors were calculated.

Introduction

Cancer is a serious health problem and is ranked as the second leading cause of mortality worldwide.[1,2] Mutation or over-expression of certain classes of signaling proteins releasing the natural cellular control leads to cancer development. RTKs (receptor tyrosine kinases) are one of the most important extracellular signaling mediators that are known to be frequently mutated in cancer. The mammalian genome contains 56 RTKs that can be subdivided into 20 different families based on their structures.[3,4]

FLT3 (FMS-like tyrosine kinase 3) is a receptor tyrosine kinase that is essential for immune response and stem cell proliferation and present in both normal and malignant lymphohematopoietic cells and. It is one of the most frequently altered genes in acute myeloid leukemia. Recently FLT3 targeted tyrosine kinase inhibitors (TKIs) have attracted a lot of interest as targeted therapeutic agents because they exert a significant cytotoxic effect on cancer cells.[5]

Since RTKs overexpression or oncogenic mutation is common in cancers, several RTKs inhibitors targeting FLT3 have become an attractive approach for the treatment of AML such as midostaurin (Rydapt, also known as PKC-412),[6] lestaurtinib (CEP-701),[7] tandutinib (MLN518),[8] dovitinib (TKI258, CHIR258),[9] sunitinib (Sutent),[10] ponatinib (Iclusig),[11] sorafenib (Nexavar),[12] and amuvatinib (MP-470)[13] which were used as first-generation FLT3 inhibitors.[14] Although many of these inhibitors had undergone preclinical and clinical trials and showed promising results, they lacked sensitivity and selectivity, hence, second-generation inhibitors, such as gilteritinib (ASP2215),[15] quizartinib (AC220),[16] and crenolanib,[17] have been approved[5,18] (Fig. 1).

On the other hand, in recent years, there has been a lot of interest in the chemotherapeutic activities of pyrazolopyrimidines as antimicrobial,[19] antiviral,[20] anti-inflammatory,[21] and potential anticancer agents.[22] Also pyrazolopyrimidines show their anticancer activity by inhibiting a variety of enzymes such as cyclin-dependent kinase,[23] Src and Abl tyrosine kinase,[24,25] glycogen synthase kinase-3,[26] adenosine deaminase,[27] epidermal growth factor receptor protein tyrosine kinase[28] and FMS-like tyrosine kinase 3 (ref. 29 and 30) (Fig. 2).

Due to these facts, and in order to find novel lead structures with potential chemotherapeutic activities, it was rationalized to design, synthesize and study the antitumor activity of some new compounds comprising the pyrazolo[3,4-*d*]pyrimidine as the main scaffold and to design these novel compounds, the following modifications were made to the reported lead compound (Fig. 3).

[a]*Pharmaceutical Organic Chemistry Department, Faculty of Pharmacy, October University for Modern Sciences and Arts (MSA), Giza, Egypt. E-mail: rmshaban@msa.edu.eg*

[b]*Pharmaceutical Chemistry Department, Faculty of Pharmacy, Ain Shams University, Abbassia, Cairo 11566, Egypt. E-mail: khaled.abouzid@pharma.asu.edu.eg*

[c]*Pharmaceutical Chemistry Department, Faculty of Pharmacy, Cairo University, Cairo, Egypt*

† Electronic supplementary information (ESI) available. See DOI: https://doi.org/10.1039/d3ra00446e

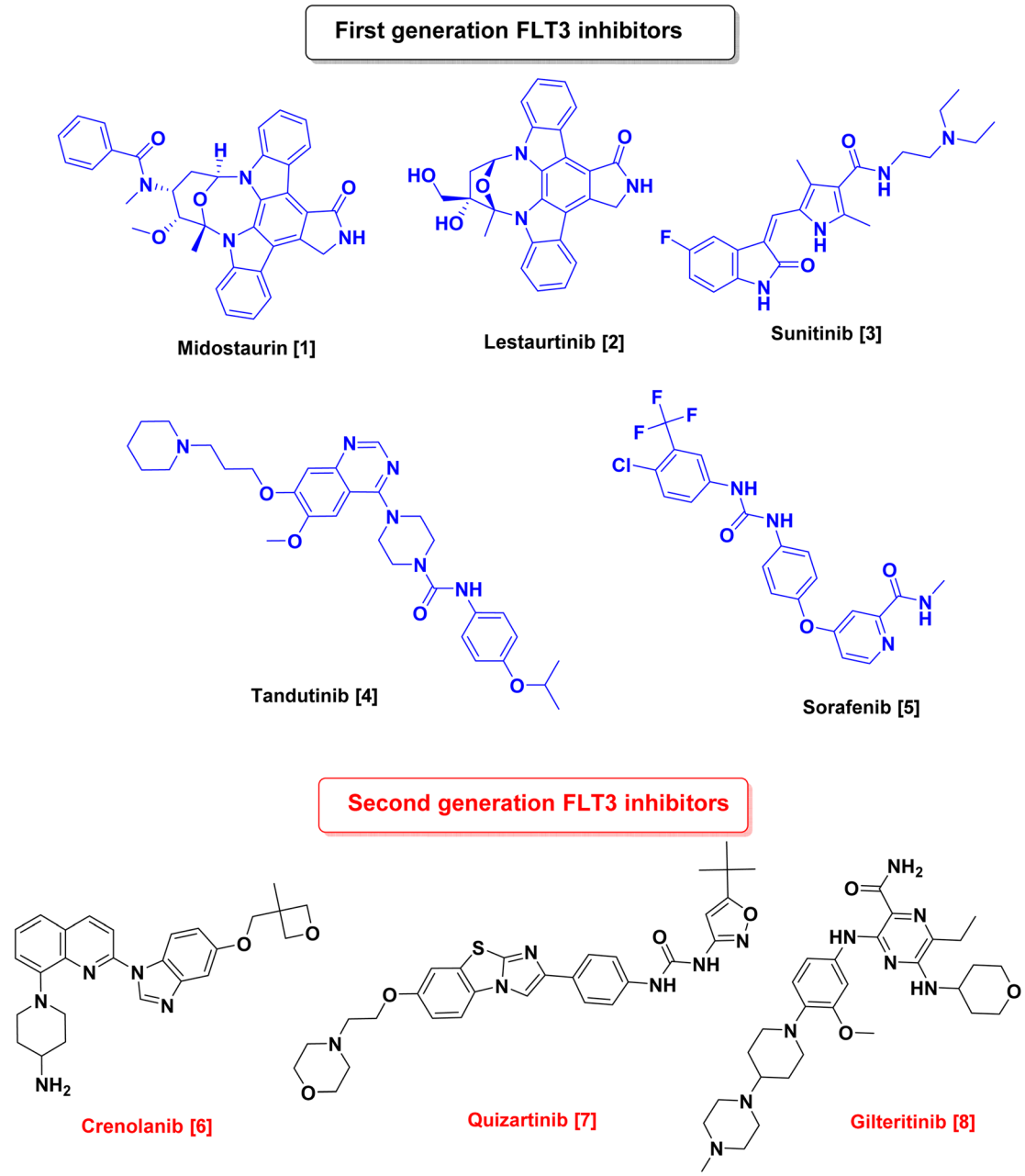

Fig. 1 Chemical structures of first & second-generation FLT3 inhibitors.

(1) The red area represents the hinge region in which the quinazoline ring was replaced by 1*H*-pyrazolo[3,4-*d*]pyrimidine because it is considered to be an isostere of purine so it can achieve a promising anti-cancer activity. The main scaffold is the critical inhibitor interacting group, which is responsible for the hydrogen bond with Cys 694 in the hinge region.

(2) The purple area contains a piperazine ring as a linker which was kept the same as the lead compound.

(3) The blue area represents the hydrogen bond region where the urea carbonyl or amide carbonyl accepts a hydrogen bond from the NH found in aspartate and the NH from the urea or amide forms a hydrogen bond to the side chain of the conserved glutamate. This area could be an amide, ester, thiourea, or aroyl isothiocyanates.

(4) The pink area represents the allosteric binding site which contains different aromatic moieties either substituted by electron-donating, electron-withdrawing, or unsubstituted to study their effect on the activity.

(5) The green area represents an unnecessary large fragment which was replaced by a simple phenyl ring in the newly synthesized compounds.

Results and discussion

Chemistry

The synthetic pathways used for the preparation of the intermediates and target products are outlined in Schemes 1–3. Scheme 1, started by reacting phenylhydrazine **VI** with ethyl 2-

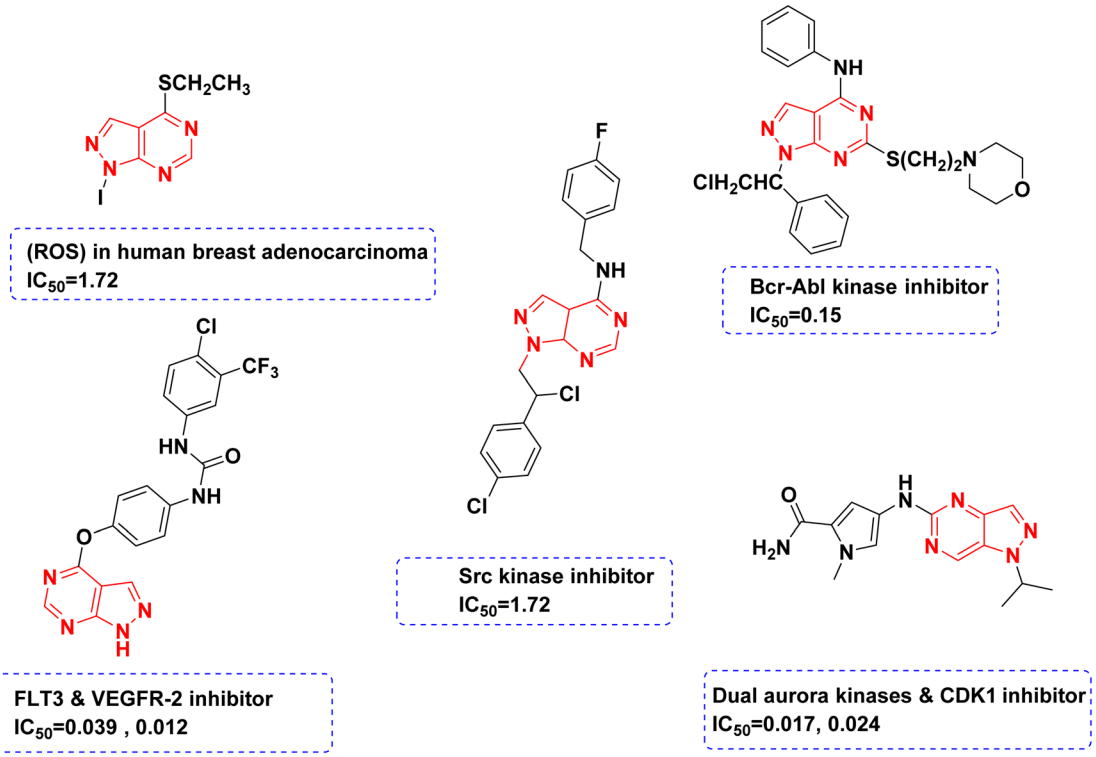

Fig. 2 Structures of different reported compounds containing pyrazolo[3,4-*d*]pyrimidine scaffold as antitumor agents with their corresponding IC_{50} in μM.

cyano-3-ethoxyacrylate **VII** to give ethyl 5-amino-1-phenyl-1*H*-pyrazolo-4-carboxylate **VIII**.[31] Cyclization of compound **VIII** was afforded *via* its reflux with formamide to yield 1-phenyl-1,5-dihydro-4*H*-pyrazolo[3,4-*d*]pyrimidin-4-one **IX**.[32] After that chlorination of compound **IX** was carried out by reflux in $POCl_3$ followed by a coupling reaction with excess anhydrous piperazine (ratio 1 : 10) in isopropanol to obtain the key intermediate **XI**.[33]

In Scheme 2, the starting intermediates **IIa–f**, **III**, **IV** & **V** were prepared *via* the reaction of chloroacetyl chloride (**I**) with aniline derivatives to give **IIa–f**.[34–36] Similarly, precursor **III** was prepared by reacting chloroacetyl chloride with α-naphthol. Also, compound **IV** was prepared by reacting chloroacetyl chloride with phenol.[37] Reacting chloroacetyl chloride with 1,3,4-thiadiazol-2-amine yields intermediate **V** (Scheme S1) (ESI†).

Final compounds **XIIa–f**, **XIII**, **XIV** & **XVI** were synthesized *via* a nucleophilic substitution reaction of intermediates **IIa–f**, **III**, **IV** & **V** respectively with the key intermediate **XI**. The ^{1}H NMR spectra for compounds **XIIa–f** & **XVI** showed one signal appeared downfield corresponding to the D_2O exchangeable proton of the NH group in the range of δ (9.70–9.99 ppm). Also, appearance of a new singlet signal in the range of δ (2.71–3.25 ppm) referring to $-CH_2$ protons. An extra singlet signal corresponding to the methyl protons for compounds **XIIe**, **XIIf** respectively appeared at δ 2.26, 2.69 ppm, and a singlet signal at δ 3.73 ppm attributed to the methoxy protons for compound **XIId**. Compounds **XIIe**, **XIIf** showed appearance of a singlet signal corresponding to CH_3 at δ 20.92 ppm. Also, an extra signal corresponding to $-OCH_3$ at δ 55.64 ppm for compound **XIId**. FT-IR spectra displayed the amidic carbonyl group (C=O) in the range of 1670–1695 cm^{-1}. ^{1}H NMR of compound **XIIa** & **XIV** showed disappearance of NH signal, and a singlet signal referring to $-CH_2$ aliphatic at δ 4.27 ppm. Moreover, compound **XV** was obtained *via* nucleophilic addition reaction of isothiocyanate derivative with intermediate **XI**. ^{1}H NMR spectra showed appearance of new signals for aromatic protons of the additional aromatic ring and a singlet signal appeared downfield corresponding to the D_2O exchangeable proton of urea group at δ 9.83 ppm. On the other hand, the synthesis of compounds **XVIIIa–f**, initially involved reacting chloroacetyl chloride with **XI**, to afford the intermediate **XVII** which was stirred at room temperature with amine derivatives to yield **XVIIIa–f**. ^{1}H NMR of compounds **XVIIIa–f** showed 1 singlet NH signal in the range of δ (5.51–6.79 ppm) which disappeared by D_2O & a singlet peak referring to $-CH_2$ aliphatic in the range of δ (2.71–3.25 ppm). Compound **XVIIId** showed an extra signal corresponding to the methoxy protons at δ 3.73 ppm. Additionally, an extra singlet signal corresponds to methyl protons for compound **XVIIIe** at δ 2.26 ppm.

Finally, in Scheme 3, the targeted compounds **XXIa–f** were synthesized by suitable several steps starting from the chlorination of benzoic acid and its derivatives with thionyl chloride to form the corresponding acid chloride **XIXa–f**. These acid chlorides were treated with ammonium thiocyanate to produce 4-un/substituted benzoyl isothiocyanates **XXa–f** which reacted

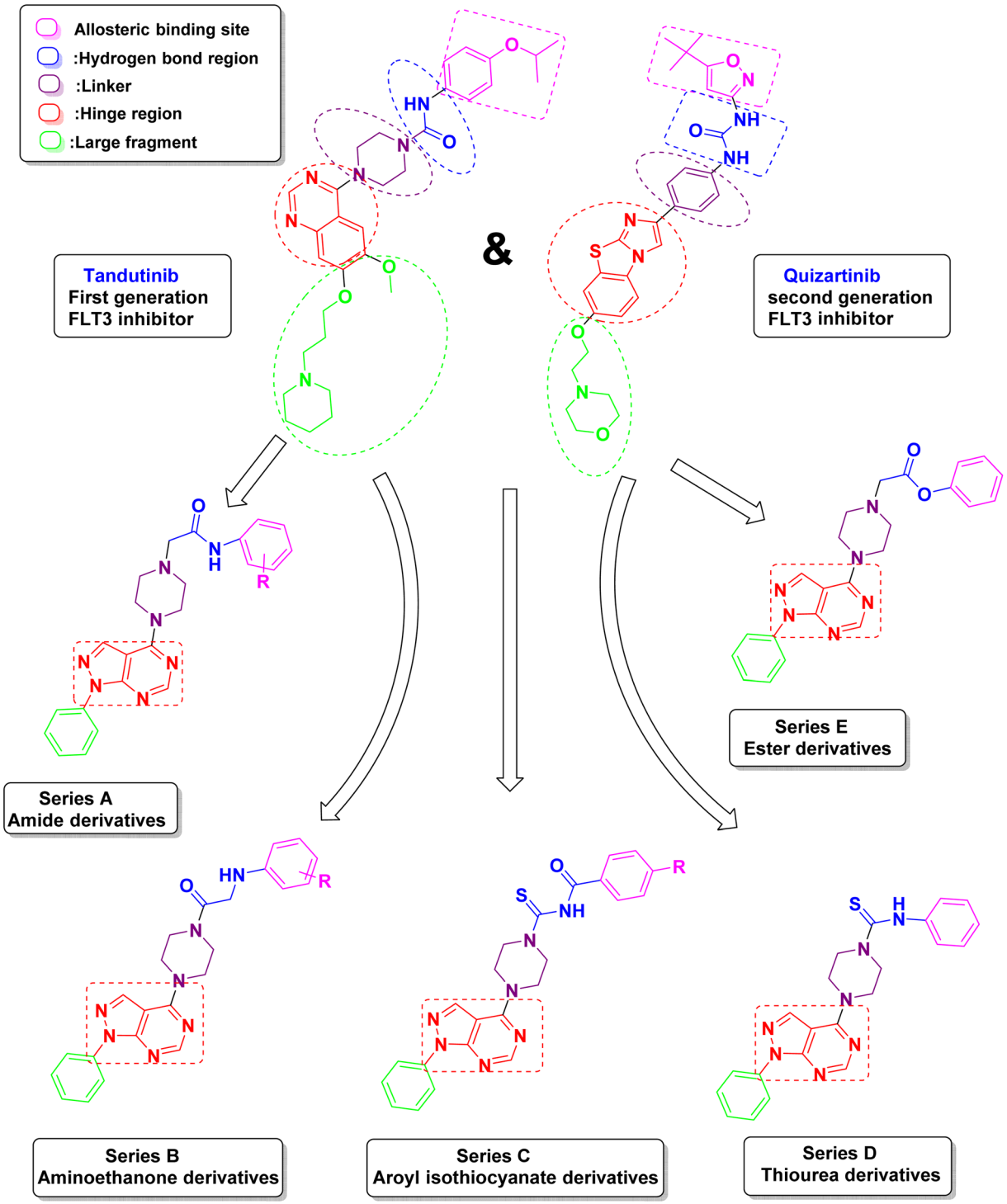

Fig. 3 Design strategy of the proposed novel pyrazolo[3,4-*d*]pyrimidine as FLT3 inhibitors.

with 1-phenyl-4-(piperazin-1-yl)-1*H*-pyrazolo[3,4-*d*]pyrimidine **XI** to give the respective aroyl isothiocyanate derivative.[38] The ^{1}H NMR spectra for compounds **XXIa–f** showed one signal appeared downfield corresponding to the D_2O exchangeable proton of NH group in the range of δ (10.80–11.12) ppm. Also, appearance of additional signals which refer to the newly formed aromatic protons. Compound **XXIe** spectrum showed a new singlet signal at δ 4.31 ppm corresponding to the methoxy protons. Compound **XXIf** spectrum showed an additional singlet signal at δ 2.39 ppm corresponding to the three protons of the methyl group. Compound **XXIf** showed an extra signal corresponding to the carbon of the methyl group at δ 20.02 ppm. Compound **XXIe** showed a new signal at δ 61.99 ppm attributed to the carbon of the methoxy group.

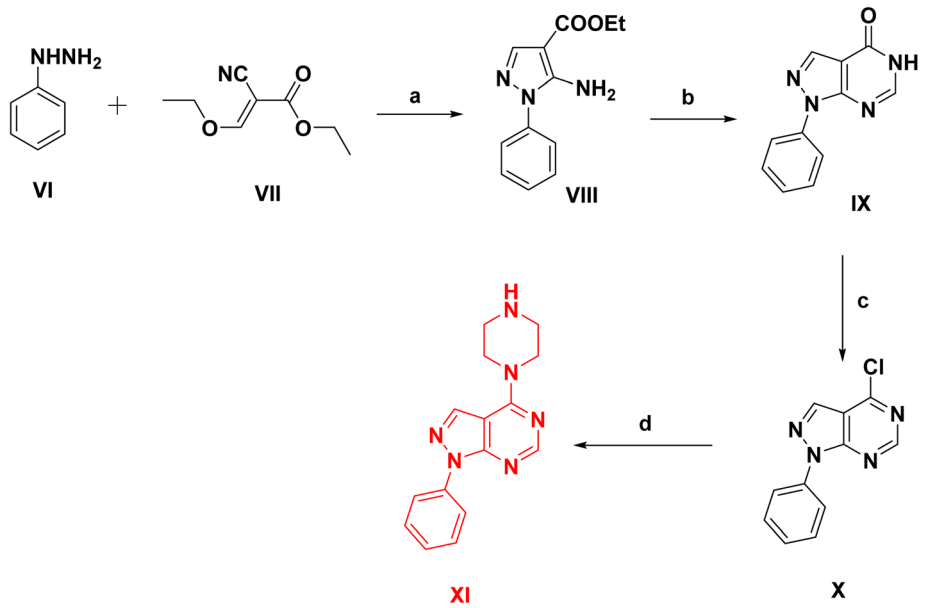

Scheme 1 Synthesis of phenyl pyrazolo-pyrimidine intermediates, reagents and conditions: (a) ethanol, reflux 6 h, 80%, (b) formamide, reflux 10 h, 70%, (c) $POCl_3$, reflux 18 h, 65%, (d) anhydrous piperazine, isopropanol, reflux 6 h, 70%.

Biological evaluation

In vitro anticancer activity against NCI-60 cell line panel

All of the designed compounds were submitted to National Cancer Institute "NCI" (https://www.dtp.nci.nih.gov), Bethesda, Maryland, USA, and all compounds were selected by the Developmental Therapeutics Program (DTP) for evaluation of their antitumor activity. The compounds were screened against 60 different human tumor cell lines, including leukemia, non-small lung cancer, colon, CNS (central nervous system), melanoma, ovarian, renal, prostate, and breast cancers at an initial single dose of 10^{-5} M concentration under the NCI drug discovery program. Furthermore, compound (**XVI**) (NSC no – 833644) showed a remarkable cell growth inhibition at 10^{-5} M so it was further screened for 5 log dose molar range.

Primary single high dose (10^{-5} M) full NCI 60 cell panel *in vitro* assay

A primary *in vitro* one-dose anticancer assay was conducted in a full NCI 60 cell panel. Results for each compound were displayed as a mean graph of the percent growth of the treated cells when compared to the untreated control cells. Analysis of the NCI-60 results showed the following:

At 10 μM concentration, compounds with the acetamide linkage **XIIa–f** & **XVI** showed the best anticancer activity among all of the tested compounds. Compound **XVI** incorporating 1,3,4-thiadiazole linked *via* piperazine acetamide linker to the parent scaffold demonstrated a highly potent inhibition percentage against most of the NCI cell panels. As it exhibited antiproliferative activity leukemia cell lines; MOLT-4 with inhibition percentages of 96.27%, colon cancer cell lines; KM12 with inhibition percentages of 95.45%, melanoma cell lines; M14 with inhibition percentages of 95.18% & MDA-MB-435 with inhibition percentages of 92.86%, breast cancer cell lines; HS 578T with inhibition percentages of 96.08%, BT-549 with inhibition percentages of 185.88% (Table 2).

Compounds **XIIa–f** incorporating a terminal un/substituted phenyl ring showed significant anticancer activity, especially against melanoma, leukemia, renal cancer & breast cancer. The broad spectrum cell inhibition was attributed to the 4-Br & 4-Cl analogs **XIIb** & **XIIc** as they exhibited antiproliferative activity against non-small cell lung cancer cell lines; NCI-H522 with inhibition percentages of 180.32, 183.09% respectively, against melanoma cell lines; MALME-3M with inhibition percentage of 154.39 & 156.24% respectively, against renal cancer cell lines; ACHN with inhibition percentage of 188.11 & 180.68% respectively, CAKI-1 with inhibition percentage of 157.01 & 139.72% respectively & UO-31 with inhibition percentage 176.96 & 160.46% respectively. Followed by 4-H & 4-CH_3 analogs **XIIe** & **XIIa** which showed good anticancer activity demonstrated in (Table 1). In addition compounds **XIIa–d** showed good anticancer activity against leukemia cell lines (MOLT-4) with percentage inhibition of 60.21%, 85.02%, 92.94% & 68.77% respectively, and a significant anticancer activity against melanoma cell lines (SK-MEL-5) with inhibition percentage of 89.62%, 90.56%, 99.65% & 71.20% respectively. Compound **XIIf** (3-CH_3 analog) didn't show any significant cell inhibition percentage except for NCI-H522 cell line as it showed an inhibition percentage 139.56% (Table 1).

Replacement of the acetamide linkage with aminoethanone linkage **XVIIIa–f** resulted in a decrease in percentage inhibition. Increased anticancer activity within this series was observed in the 4-Br, 4-Cl & 3-CH_3 analogues **XVIIIb**, **XVIIIc** & **XVIIIf** as it showed significant antiproliferative activity against non-small cell lung cancer NCI-H522 with inhibition percentage of 73.62, 50.17 & 106.93% respectively, against melanoma (SK-

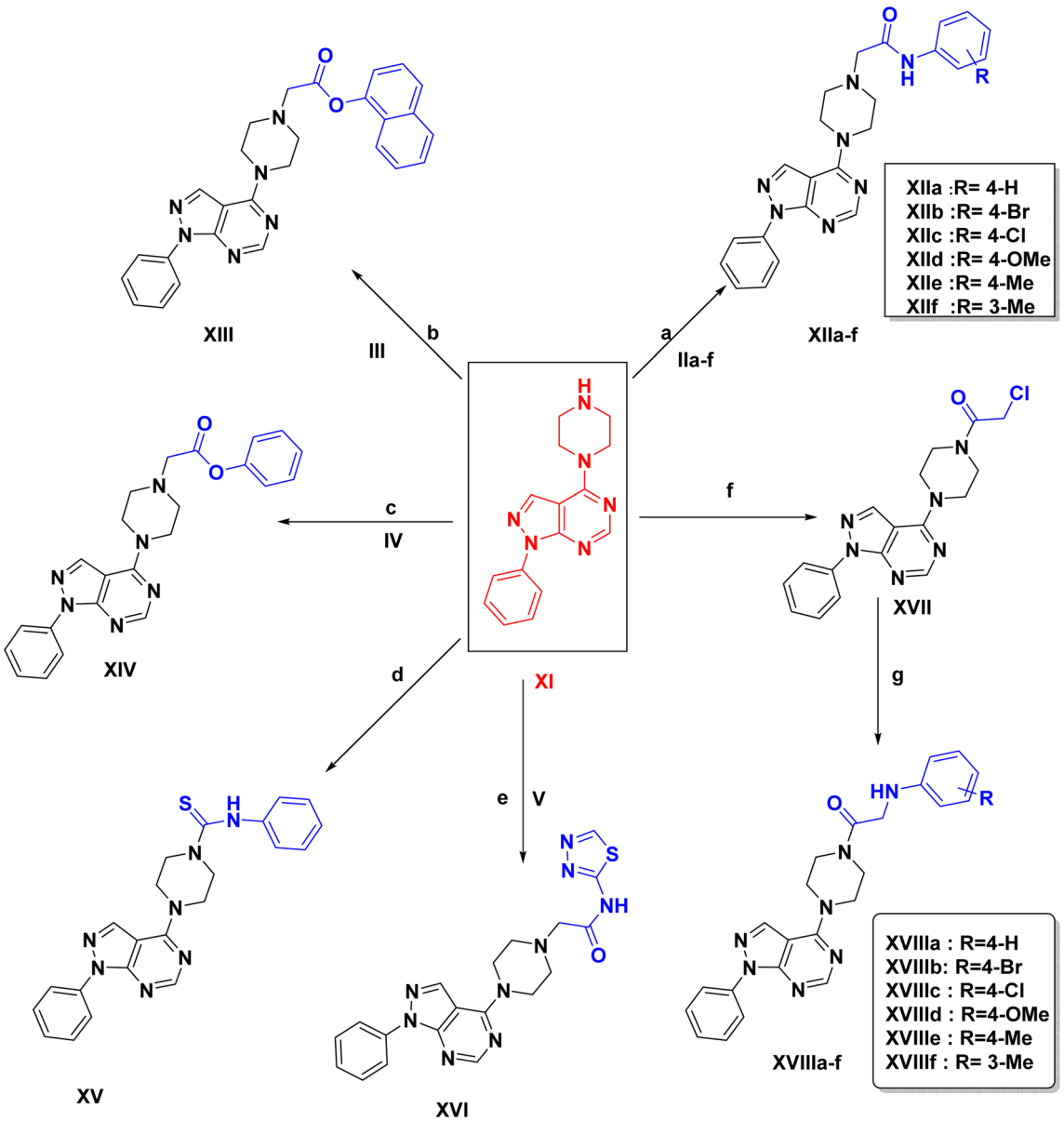

Scheme 2 Reagents and conditions: (a) $NaHCO_3$, KI, DMF, rt, 36 h, 65–83% (b) $NaHCO_3$, KI, DMF, rt, 24 h, 55–65%, (c) $NaHCO_3$, KI, DMF, rt, 24 h, 50%, (d) phenyl isothiocyanate, dry DCM, reflux, 2 h, 75%, (e) $NaHCO_3$, KI, DMF, rt, 36 h, 75%, (f) 2-chloroacetyl chloride, anhydrous sodium acetate, DMF, reflux, 16 h, 65%, (g) aromatic amine derivatives, $NaHCO_3$, KI, DMF, rt, 48 h, 62–80%.

MEL-5) with inhibition percentage of 67.48, 74.36 & 62.50 respectively, against renal cancer UO-31 with inhibition percentage 68.99, 68.08 & 65.74% respectively and against breast cancer T-47D with inhibition percentage 72.72, 63.26 & 66.43% respectively. Followed by 4-OCH_3 & 4-CH_3 analogues which showed good anticancer activity against melanoma SK-MEL-5 with inhibition percentages 83.62, 64.82% respectively and against breast cancer T-47D with inhibition percentages 74.01, 62.13% respectively (Table S1) (ESI†).

Compounds **XXIa–f** incorporating piperazine linked to *n*-aroyl thioamide showed a good anticancer activity against non-small cell lung cancer, CNS cancer & renal cancer which was demonstrated in (Table S2) (ESI†) especially compound **XXIf** which showed a remarkable activity against leukemia SR (inhibition 80.09%), against non-small cell lung cancer HOP-62 (inhibition 102.01%), HOP-92 (inhibition 85.26%), against CNS cancer SF-539 (inhibition 88.81%), SNB-19 (inhibition 71.82%), SNB-75 (inhibition 97.65%) and against renal cancer 786-0 (inhibition 72.18%), ACHN (inhibition 75.48%), CAKI-1 (inhibition 72.33%) & SN12C (inhibition 71.70%).

On contrary, compounds **XIV** & **XV** didn't show any significant cell inhibition percentage, while compound **XIII** showed significant anticancer activity against non-small cell lung cancer, NCI-H322M (inhibition 69.30%), NCI-H460 (inhibition 65.00), against colon cancer COLO 205 (inhibition 97.35%), HCC-2998 (inhibition 86.37%), HCT-15 (inhibition 72.94%),

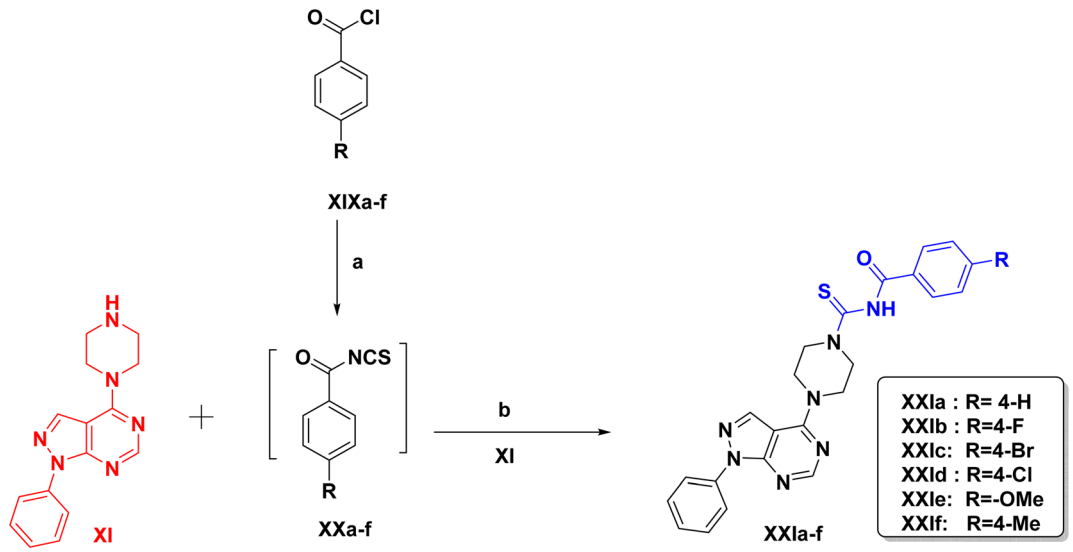

Scheme 3 Reagents & conditions: (a) ammonium thiocynate, dry acetone, vigorous stirring, rt, 45 min. (b) Dry acetone, rt, 36 h, 65–90%.

HT29 (inhibition 83.52%), against melanoma MALME-3M (inhibition 72.76%), against ovarian OVCAR-3 (inhibition 94.00%), against renal cancer 786-0 (inhibition 80.79%), A498 (inhibition 107.50%), SN12C (inhibition 76.90%), TK-10 (inhibition 93.85%) (Table 2).

The investigation of the structure–activity relationship of all the newly synthesized compounds revealed that the highest anticancer activity was observed in the series with the acetamide linkage (NHCO) (**XIIa–f**). Increasing the density of the hetero atom of the structure of (**XIIa–f**) by introducing a thiazole ring seems to enhance the activity (**XVI**) as this compound showed promising anticancer activity against most of the cell lines. *Meta* substitution on the phenyl ring diminished the activity, whereas unsubstitution and *para* substitution on the benzene ring improved the activity. This is validated by compounds containing *para* or unsubstituted phenyl (**XIIa–e**) which demonstrated promising activity in comparison to compound (**XIIf**) with 3-CH_3 which showed no significant activity. The introduction of a small electron withdrawing group such as chloro (**XIIc**, **XVIIIc**) or bromo (**XIIb**, **XVIIIb**) increases the activity while introducing an electron donating group (**XIIe**, **XVIIIe**) slightly decreases the activity. The presence of a phenyl ring seems to be essential for activity. It was predicted that increasing the ring size to the naphthyl group in compound (**XIII**) enhance the hydrophobic interaction and thus increases the activity, but, in our study, the naphthyl group has lower activity than phenyl, so we concluded that the bulkier group is not preferable.

In vitro 5 dose full NCI 60 cell panel assay

Due to the significant cell growth inhibition of compound **XVI** against a variety of cell lines, it was further screened for NCI full panel 5 dose assays. All 60 cell lines, representing nine tumor subpanels, were incubated at five different concentrations (0.01, 0.1, 1, 10, and 100 μM of compound **XVI**). In order to calculate the three response parameters (GI_{50}, TGI & LC_{50}) for each cell line, the assay results were used to create log concentration *vs.* % growth curves. GI_{50} (growth inhibitory activity) refers to the concentration of the compound causing a decrease in cell growth by 50%. Total growth inhibition or TGI, refers to the concentration of the compound resulting in total growth inhibition. LC_{50} or cytotoxic activity refers to the concentration of the compound that causes net 50% loss of initial cells at the end of 48 hours incubation period of. Compound **XVI** demonstrated remarkable antitumor activity against most of the cell lines representing nine subpanels with GI_{50} between 1.17 and 18.40 μM (Table 3).

Compound (**XVI**) showed significant activity against non-small cell lung cancer HOP-62 with GI_{50} 1.62, a TGI value of 3.29 and LC_{50} value of 6.68, HOP-92 with GI_{50} 1.57, a TGI value of 3.46 and LC_{50} value of 7.62, NCI-H522 with GI_{50} 1.62, a TGI value of 3.09 and LC_{50} value of 5.90, against melanoma LOX IMVI with GI_{50} 1.49, a TGI value of 2.81 and LC_{50} value of 5.30, MALME-3M with GI_{50} 1.69, a TGI value of 3.30 and LC_{50} value of 6.41, against ovarian cancer OVCAR-3 with GI_{50} 1.93, a TGI value of 3.67 and LC_{50} value of 6.98, against renal cancer CAKI-1 with GI_{50} 1.60, a TGI value of 2.97 and LC_{50} value of 5.54, RXF 393 with GI_{50} 1.68, a TGI value of 3.31 and LC_{50} value of 6.53, UO-31 with GI_{50} 1.17, a TGI value of 2.39 and LC_{50} value of 4.89, and against breast cancer BT-549 with GI_{50} 1.55, a TGI value of 3.02 and LC_{50} value of 5.88 (Table 3).

Molecular docking

In this study, the docking was carried out using MOE software. The molecular docking study was conducted between the newly synthesized compounds and the binding site of FLT3. Each test molecule gave 10 possible docked poses. The ideal pose of each molecule was selected according to the similarity of its binding mode in the binding site to that of the lead compound.

To validate our docking, we re-docked the selective inhibitor (quizartinib) in the FLT3 kinase domain. We compared its binding mode and interactions with interactions of the newly

Table 1 The sixty human tumor cell line anticancer screening data at single dose assay (10^{-5} M concentration) as percent cell inhibition of compounds XIIa–f[a]

	Compound no.					
Cell line	XIIa	XIIb	XIIc	XIId	XIIe	XIIf
Leukemia						
CCRF-CEM	NT	38.41	48.08	36.39	21.61	23.28
HL-60(TB)	35.49	35.69	41.41	17.31	4.62	11.66
K-562	61.47	57.25	57.65	46.40	40.15	32.50
MOLT-4	60.21	85.02	92.94	68.77	31.94	25.03
RPMI-8226	33.84	57.43	55.63	45.31	24.17	24.81
SR	45.61	59.65	63.12	44.98	47.42	44.11
Non-small cell lung cancer						
A549/ATCC	13.93	24.81	33.00	14.49	10.91	2.99
EKVX	37.47	53.14	54.99	45.12	18.97	14.09
HOP-62	20.79	15.43	14.26	11.63	4.42	3.77
HOP-92	27.73	25.37	30.21	28.33	9.06	1.79
NCI-H226	36.03	37.52	32.46	24.13	23.53	15.23
NCI-H23	49.27	NT	NT	NT	NT	NT
NCI-H322M	18.12	22.82	21.07	11.51	13.48	8.67
NCI-H460	23.75	42.31	46.71	20.68	25.97	26.99
NCI-H522	41.99	180.32	183.09	37.64	141.06	139.56
Colon cancer						
COLO 205	3.66	29.42	43.32	13.25	−10.90	−9.41
HCC-2998	1.69	21.22	44.23	−10.65	−2.01	−7.15
HCT-116	45.12	47.55	48.15	25.62	23.71	41.36
HCT-15	43.02	54.83	54.97	40.95	49.75	44.65
HT29	16.07	26.71	36.56	12.80	6.16	23.90
KM12	28.82	42.50	46.85	25.04	10.08	9.58
SW-620	13.30	21.88	21.63	2.27	0.11	8.02
CNS cancer						
SF-268	17.75	41.16	55.72	26.14	19.35	11.56
SF-295	45.05	17.02	19.73	−2.88	−15.82	−17.04
SF-539	13.14	17.69	23.93	6.04	15.44	−1.83
SNB-19	26.69	30.71	33.50	16.22	14.09	16.89
SNB-75	37.81	19.11	30.34	−0.02	−3.25	−0.44
U251	16.85	23.83	33.26	14.59	13.49	10.99
Melanoma						
LOX IMVI	32.63	18.24	60.12	30.94	76.75	11.85
MALME-3M	38.46	154.39	156.24	1.18	9.24	0.56
M14	28.65	40.68	40.60	18.49	−0.21	5.60
MDA-MB-435	36.50	46.78	52.99	22.24	5.77	6.60
SK-MEL-2	61.99	70.09	65.82	46.01	12.24	19.83
SK-MEL-28	13.59	28.02	27.24	5.38	13.51	9.89
SK-MEL-5	89.62	90.56	99.65	71.20	22.37	21.54
UACC-257	32.44	41.35	50.08	24.51	7.22	−1.73
UACC-62	51.52	54.90	54.66	50.43	30.67	32.10
Ovarian cancer						
IGROV1	50.14	41.88	51.98	43.20	18.74	16.12
OVCAR-3	16.99	39.45	48.21	30.54	−3.49	1.05
OVCAR-4	58.25	43.54	55.54	36.54	17.13	8.65
OVCAR-5	6.29	21.80	14.40	5.17	2.05	5.28
OVCAR-8	26.00	35.31	43.36	27.07	28.63	3.97
NCI/ADR-RES	36.74	43.85	51.95	30.40	20.48	10.59
SK-OV-3	29.90	23.31	20.77	8.64	−12.48	0.27
Renal cancer						
786-0	1.86	161.68	59.55	−1.53	−4.76	1.95
A498	5.96	9.14	21.35	−1.31	−4.13	2.01
ACHN	36.75	188.11	180.68	34.31	132.69	20.13

Table 1 (*Contd.*)

	Compound no.					
Cell line	**XIIa**	**XIIb**	**XIIc**	**XIId**	**XIIe**	**XIIf**
CAKI-1	39.43	157.01	139.72	34.58	22.23	17.12
RXF 393	14.49	24.02	25.56	5.14	13.26	9.98
SN12C	22.41	60.92	53.38	31.70	25.36	16.62
TK-10	−17.93	−20.84	2.70	−29.22	−51.91	−30.21
UO-31	63.03	176.96	160.46	57.85	36.99	45.05
Prostate cancer						
PC-3	30.30	50.94	61.20	41.03	34.48	36.86
DU-145	21.60	32.14	42.52	21.09	7.47	3.28
Breast cancer						
MCF7	60.38	63.24	72.43	52.81	25.80	25.18
MDA-MB-231/ATCC	26.94	33.31	36.66	24.57	19.43	12.65
HS 578T	22.07	29.25	35.36	19.42	22.28	11.82
BT-549	46.33	49.95	60.86	46.27	14.96	10.12
T-47D	73.06	58.43	73.32	69.54	21.08	27.85
MDA-MB-468	85.22	50.81	57.49	46.51	12.93	10.77
Mean	66.84	48.34	45.02	74.12	81.11	85.10

[a] NT, not tested.

synthesized pyrazolo[3,4-*d*]pyrimidine derivatives. Quizartinib binds to the crystal structure of the FLT3 kinase domain (PDB code: 4RT7) through different amino acids. The benzo(*d*)imidazo[2,1-*b*]thiazole forms 1 hydrogen bond with Cys 694 & fits into the hinge region. In the allosteric site, there are two essential interaction of the urea moiety with the protein; the NH makes a hydrogen bond with Glu 661 while the carbonyl group of urea interacts with Asp 829 (Fig. 4 and 5).

Compounds with amide linkage **XIIa–f** fulfilled all of the essential features as done by the lead compound in the FLT3 ATP binding site as they formed one hydrogen bond with Cys 694 in the hinge region and two hydrogen bonds with Glu 661, Asp 829 in the allosteric binding site, this could explain the high anti-cancer activity of these compounds except for compound **XIIa** that binds only with Cys 694 in the hinge region. One of the best-scored poses is presented in Fig. 6.

Compound **XVI** lost the binding interaction with Asp 829 in the allosteric binding site (Fig. 7). Compounds **XVIIa–f**, **XIII**, **XIV** & **XV** fulfilled the binding interaction in the hinge region but binds only with Asp 829 in the allosteric binding site, except for compound **XVIIIC** lost the binding interaction with the main amino acid (Cys 694) in the hinge region, resulting in lower docking scores which explains the lower anticancer activity in comparison with compounds with the amide linkage **XIIa–f** (Fig. 6). Finally, compounds **XXIa–f** lost the binding interaction in the allosteric binding site and formed an additional hydrogen bond with Lys 644.

In vitro enzyme inhibition assay

In an attempt to investigate the possible mechanism of action of all the synthesized compounds based on the structural similarities with tandutinib and quizartinib, all of them were evaluated for their FLT3 inhibitory activity at Thermo Fisher Scientific, USA (**https://www.thermofischer.com/selectscreen**). The assay was conducted using the Z′-LYTE biochemical assay which applies a fluorescence-based, coupled-enzyme method. All of the compounds were tested against FLT3 in a single-point concentration assay at 10 μM to measure their inhibition percentage. Unfortunately, the targeted compounds showed weak inhibitory activity against FLT3, where most of the compounds activity was between 5% and 29%. Because of these results, an additional investigation was performed to understand the low activity of the synthesized compounds as described next (Table 4).

Molecular dynamics (MD)

Even though the targeted compounds had structural similarities with tandutinib and quizartinib, they fulfilled most of the key interactions as done by the lead compound in molecular docking, moreover, they showed significant antiproliferative activity against most of the cell lines in NCI sixty cell panel, they showed low enzymatic activity against FLT3 so to understand these findings, molecular dynamics was performed to gain more insight into the binding mode of 4RT7, molecular dynamics simulations were performed on the docked complexes of the highest-ranked docking compounds with the highest percentage of enzyme inhibition against FLT3 kinase domain **XIIb**, **XIIc** & **XVI**. Quizartinib was also subjected to MD simulations to account for its binding mode and protein dynamics as a reference, resulting in a total of four MD runs. MD was carried out for 50 ns at NPT ensemble (constant number of particles, pressure, and temperature), for minimization and equilibration purposes. Various computational techniques such as RMSD, RG, RMSF, and H-bond analysis were

Table 2 The sixty human tumor cell line anticancer screening data at single dose assay (10^{-5} M concentration) as percent cell inhibition of compounds XIII, XIV, XV & XVI[a]

	Compound no.			
Cell line	**XIII**	**XIV**	**XV**	**XVI**
Leukemia				
CCRF-CEM	4.35	14.88	−3.11	NT
HL-60(TB)	3.30	10.45	1.88	145.54
K-562	2.63	25.34	−0.25	89.44
MOLT-4	0.73	11.59	−7.57	96.27
RPMI-8226	3.55	24.02	0.80	116.64
SR	6.80	26.04	4.74	128.89
Non-small cell lung cancer				
A549/ATCC	−9.39	−5.50	−6.49	132.54
EKVX	12.37	17.80	5.12	144.79
HOP-62	−2.98	−3.48	5.00	152.69
HOP-92	−6.68	4.35	4.93	170.93
NCI-H226	11.49	32.35	17.11	56.09
NCI-H23	NT	NT	NT	155.11
NCI-H322M	69.30	10.33	1.59	15.17
NCI-H460	65.00	3.85	−6.06	122.10
NCI-H522	−6.93	20.20	10.84	179.35
Colon cancer				
COLO 205	97.35	−4.70	−7.70	150.21
HCC-2998	86.37	−6.65	−3.24	40.29
HCT-116	58.65	8.74	−9.85	91.77
HCT-15	72.94	2.34	−11.65	130.72
HT29	83.52	−1.02	−4.77	161.53
KM12	40.60	9.07	2.76	95.45
SW-620	81.53	3.20	−1.88	123.86
CNS cancer				
SF-268	73.30	8.83	6.94	134.37
SF-295	46.58	−11.73	−9.76	131.40
SF-539	59.89	2.29	−3.61	188.20
SNB-19	88.90	1.89	−1.52	41.60
SNB-75	53.50	−8.62	19.30	174.96
U251	87.14	2.45	−0.28	172.52
Melanoma				
LOX IMVI	53.82	21.59	11.67	187.39
MALME-3M	72.76	0.21	−10.37	167.26
M14	62.16	3.99	−5.15	95.18
MDA-MB-435	58.98	3.15	−3.11	92.86
SK-MEL-2	46.66	8.32	−5.97	72.03
SK-MEL-28	59.00	4.21	−4.39	27.65
SK-MEL-5	37.50	27.16	5.86	70.64
UACC-257	66.91	−3.73	−10.30	45.74
UACC-62	34.57	18.17	3.34	82.55
Ovarian cancer				
IGROV1	59.41	10.34	49.06	141.81
OVCAR-3	94.00	12.46	−5.47	155.56
OVCAR-4	51.61	8.69	0.64	86.42
OVCAR-5	83.82	3.43	−1.45	104.09
OVCAR-8	65.24	5.72	0.41	121.38
NCI/ADR-RES	60.62	8.96	−0.12	132.63
SK-OV-3	67.09	1.90	−10.10	71.86
Renal cancer				
786-0	80.79	0.36	5.63	180.94
A498	107.50	−4.72	3.13	51.04
ACHN	45.35	20.47	9.38	187.46
CAKI-1	47.75	21.68	28.23	195.69
RXF 393	76.34	4.44	−10.84	171.34
SN12C	76.90	17.97	3.48	154.68
TK-10	93.85	−34.09	−15.74	156.49
UO-31	34.26	45.53	31.93	197.16
Prostate cancer				
PC-3	70.01	19.04	10.97	136.14
DU-145	75.39	−1.94	−5.36	196.08
Breast cancer				
MCF7	45.57	27.53	16.49	83.90
MDA-MB-231/ATCC	64.96	6.69	−0.80	70.26
HS 578T	60.40	12.15	9.50	96.08
BT-549	76.87	13.66	0.30	185.88
T-47D	33.57	30.68	20.07	72.12
MDA-MB-468	35.78	31.66	2.52	139.82
Mean	94.47	90.78	97.85	−23.26

[a] NT, not tested.

used to analyze the structural changes and dynamic behavior in complexes (Fig. 8).

To monitor structural and conformational changes, RMSD analysis was carried out. RMSD (root mean square deviation) is used to measure the stability of the protein–ligand complex as it measures the average distance between a group of atoms. The stability for each compound was compared to that of quizartinib as a reference over the trajectory of 50 ns. The RMSD for the ligand in each trajectory is plotted against simulation time in ns and illustrated in (Fig. 9). RMSD of the protein backbone (Cα, C, and N) in the 4 dynamics runs show stability after 10 ns of the simulation with RMSD 1.24 ± 0.12, 1.08 ± 0.15, 1.18 ± 0.12 and 1.41 ± 0.13 Å (mean ± SD) for **XIIb**, **XIIc**, **XVI**, and quizartinib respectively. Low RMSD values (1–2 Å) indicate the stability of the protein–ligand complex. Compounds **XIIc** & **XVI** showed a slight fluctuation at 10 & 50 ns respectively, it seems that the ligand tries to explore other conformations but they remain stable for the rest of the simulation. In conclusion, the RMSD fluctuation analysis suggests that the MD trajectories were overall stable complex (Fig. 10).

RMSF (root mean square fluctuation) was used to calculate the average fluctuation of each amino acid of the protein. RMSF values appear to be relatively high (> 2 Å) in the regions of amino acids 25–50, 160 & 270 for compounds **XIIc** & **XVI** which indicates that they are terminal or far away from the binding site; hence this may affect their biological activity. The rest of the binding site amino acids showed lower RMSF values (<2 Å) indicating their stability during the simulation.

The radius of gyration (R_g) is a measure of the compactness of the protein during the simulation. As shown in (Fig. 11), R_g values of **XIIb**, **XIIc**, **XVI** & reference were 19.25 ± 0.10, 19.27 ±

Table 3 NCI *in vitro* testing result of compound XVI at five dose level in μM

Pannel	Cell line	GI_{50}	TGI	LC_{50}
Leukemia	CCRF-CEM	*2.55*	7.17	100
	HL-60(TB)	10.40	39.50	100
	K-562	7.91	36.60	100
	MOLT-4	*4.08*	31.30	100
	RPMI-8226	*2.83*	8.67	62.8
	SR	*2.11*	5.26	100
Non-small cell lung cancer	A549/ATCC	*2.07*	4.31	9.01
	EKVX	*2.90*	11.10	39.90
	HOP-62	*1.62*	3.29	6.68
	HOP-92	*1.57*	3.46	7.62
	NCI-H226	*1.84*	5.14	43.90
	NCI-H23	*1.74*	3.57	7.33
	NCI-H322M	14.40	27.50	52.40
	NCI-H460	*4.25*	14.70	41.30
	NCI-H522	*1.62*	3.09	5.90
Colon cancer	COLO 205	14.04	27.00	52.00
	HCC-2998	13.60	26.00	51.40
	HCT-116	*3.75*	14.50	38.10
	HCT-15	*1.79*	3.42	6.55
	HT29	6.91	19.30	43.90
	KM12	*4.46*	15.90	39.90
	SW-620	*4.99*	16.10	40.10
CNS cancer	SF-268	*4.79*	19.30	59.60
	SF-295	10.30	22.30	48.20
	SF-539	*1.76*	3.32	6.26
	SNB-19	12.20	24.60	49.60
	SNB-75	15.10	30.50	16.50
	U251	*1.92*	3.99	8.27
Melanoma	LOX IMVI	*1.49*	2.81	5.30
	MALME-3M	*1.69*	3.30	6.41
	M14	*4.17*	16.20	40.30
	MDA-MB-435	13.60	27.50	55.30
	SK-MEL-2	12.60	25.80	52.80
	SK-MEL-28	13.90	26.90	51.90
	SK-MEL-5	10.20	21.90	46.80
	UACC-257	14.10	28.10	56.20
	UACC-62	*4.97*	18.70	43.30
Ovarian cancer	IGROV1	*2.68*	7.65	29.50
	OVCAR-3	*1.93*	3.67	6.98
	OVCAR-4	10.30	28.10	76.70
	OVCAR-5	6.41	19.30	44.00
	OVCAR-8	*1.93*	4.02	8.38
	NCI/ADR-RES	*1.77*	3.69	7.72
	SK-OV-3	*1.25*	25.00	50.00
Renal cancer	786-0	*1.99*	3.56	6.37
	A498	18.40	35.00	6.67
	ACHN	*1.79*	3.18	5.64
	CAKI-1	*1.60*	2.97	5.54
	RXF 393	*1.68*	3.31	6.53
	SN12C	*1.94*	5.06	16.80
	TK-10	*3.09*	6.14	16.80
	UO-31	*1.17*	2.39	4.89
Prostate cancer	PC-3	*4.33*	17.10	44.40
	DU-145	*1.80*	3.24	5.82
Breast cancer	MCF7	*4.32*	18.00	47.70
	MDA-MB-231/ATCC	*1.78*	3.87	8.41
	HS 578T	12.40	63.00	100.00
	BT-549	*1.55*	3.02	5.88
	T-47D	7.93	24.10	62.80
	MDA-MB-468	*3.06*	13.80	44.10

0.11, 19.29 ± 0.56, and 19.15 ± 0.77 Å (mean ± SD), respectively. R_g is stable for each protein throughout the simulation; hence, no major conformational changes occur during the simulation.

Hydrogen bonding analysis between each compound and the protein was performed to investigate the hydrogen bonding contribution to the overall binding interactions. (Fig. 12) describes the number of H-bonds formed during the simulation time. The reference compound (quizartinib) shows the highest number of H-bonds to the protein which indicates its strong binding. This also reflects its high docking score. On the other hand, compounds **XIIb**, **XIIc**, and **XVI** show a lower number of formed H-bonds when compared to the reference, also these compounds do not seem to form any stable H-bonds with the three essential amino acids as the lifetime of hydrogen bond was very low (Table 5) which indicate their weaker binding, which can reflect their low enzymatic activity in the biological evaluation.

In silico predictive ADME study for targeted compounds

In an attempt to further examine the pharmacokinetics properties of synthesized compounds, a computer-aided ADMET study was conducted by using Accelrys Discovery Studio 2.5 software. These studies were based on various molecular descriptors and involved the calculation of some parameters as atom-based log *P*98 (*A* log *P*98), aqueous solubility level (AQ SOl LEV), 2D polar surface area (ADMET 2D PSA), blood–brain barrier level (BBB LEV), cytochrome P450 2D6 (CYP2D6), hepatotoxicity level (HEPATOX LEV) and hepatotoxicity probability (HEPATOX PROB). All the calculated parameters are tabulated in (Table 6). The results of the ADMET study are presented as ADMET 2D plot drawn using calculated PSA_2D and *A* log *P*98 properties (Fig. 13).

Blood–Brain Barrier (BBB) and Human Intestinal Absorption (HIA) plots (Fig. 13) were drawn using all the compounds. In the BBB plot, compound **XVI** falls outside the 99% confidence ellipse (undefined), whereas the rest of the compounds fall inside the 95–99% ellipse. Hence, compound **XVI** may have very low penetration to the blood–brain barrier, therefore it may have a low chance for CNS side effects. On the contrary, the rest of the compounds may have a medium to high degree of penetration so these compounds may be good candidates for brain tumors. In the HIA plot, all compounds fall inside the 99% ellipse. Hence, they are predicted to possess good human intestinal absorption with an absorption level 0.

The aqueous solubility level was predicted to be one or two which indicates very low aqueous solubility. The ADME HEPATOTOX.PROB values of most of the compounds range from 0.15–0.40 with hepatotoxicity level 0 which is considered to be not toxic. The CYP2D6 value predicts the inhibitory and non-inhibitory aspects of the titled chemical structure on cytochrome P450 2D6 enzyme. Most of the compounds are foreseen as inhibitors of CYP2D6, so drug–drug interactions are expected upon administration of these compounds. Seven compounds are predicted as non-inhibitor for CYP2D6, so side effects such as liver dysfunction are not expected upon administration of these compounds.[39]

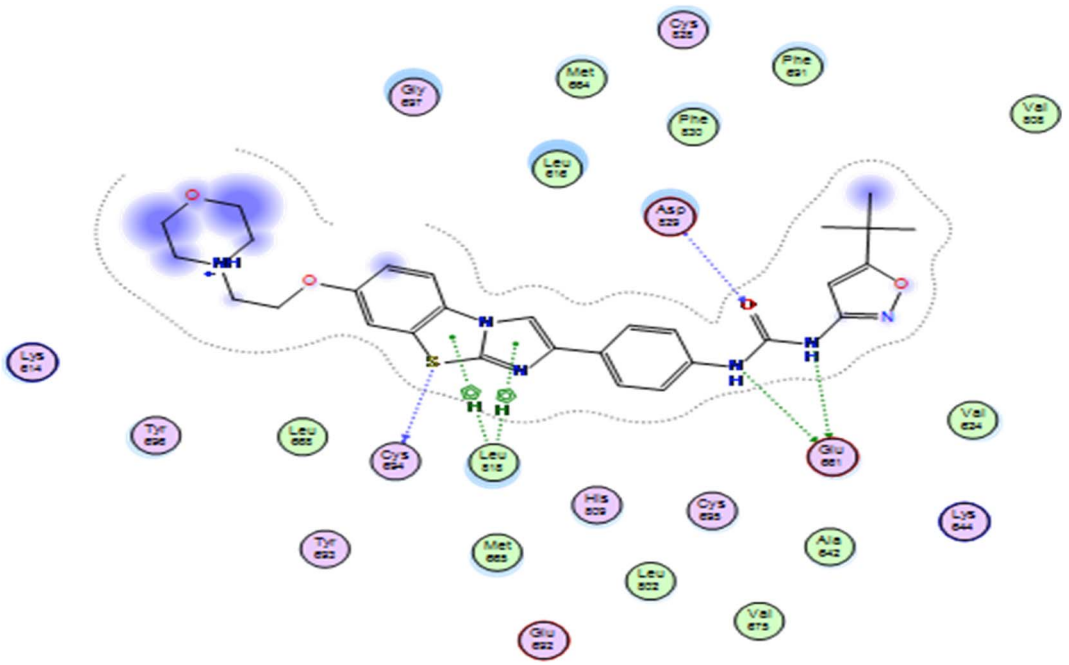

Fig. 4 2D representation of quizartinib (re-docked) in FLT3 kinase binding domain (PDB code: 4RT7), showing the same key interactions as reported.

PSA is an important property that is associated with the drug bioavailability. Thus, molecules that are passively absorbed with PSA > 140 thought to have low bioavailability. All the synthesized compounds have PSA ranging from 58.64–98.46, thus theoretically they should show good passive oral absorption.

Conclusion

In the present study, a novel 21 compounds of pyrazolo[3,4-*d*] pyrimidine derivatives were designed and synthesized based on their structural similarities with tandutinib and quizartinib. Their structures were confirmed by various spectral and micro analytical data (^{1}H NMR, ^{13}C NMR, FT IR, mass spectrum, elemental analyses, and high resolution mass). Moreover, compounds were biologically evaluated for their antiproliferative activity against NCI sixty cell line panels as well as *in vitro* FLT3 inhibitory activity.

Out of the titled compounds, compound **XVI** was further screened for NCI full panel 5 dose assays and demonstrated a remarkable anticancer activity against most of the cell lines representing nine subpanels. Additionally, compounds with the piperazine acetamide linkage bearing a terminal substituted phenyl ring **XIIa–f** exhibited a significant anticancer activity at 10 μM concentration, particularly against melanoma, leukemia, renal cancer, and breast cancer. Molecular docking studies were conducted to investigate the effect of our compounds on FLT3 and revealed the ability of piperazine acetamide based derivatives to fulfill all the key features as done by the lead compound. However, other compounds missed a key interaction, resulting in lower docking scores. Unfortunately, all compounds showed a weak *in vitro* FLT3 inhibitory activity which couldn't explain

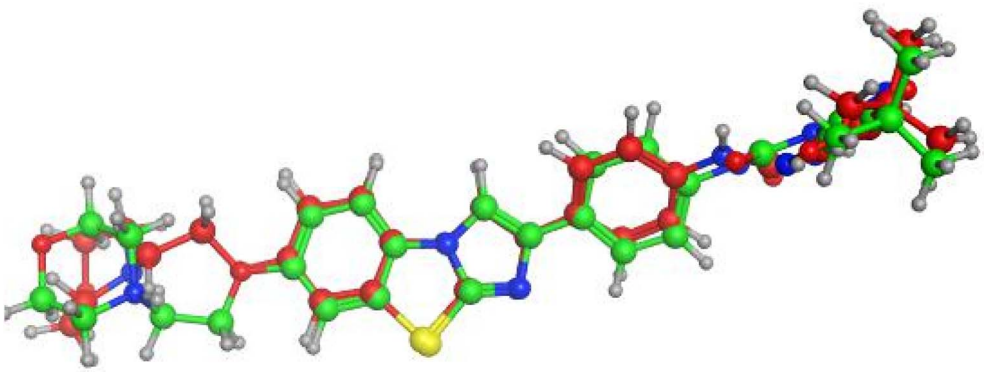

Fig. 5 Alignment of the original ligand quizartinib (green) and re-docked ligand (red) at FLT3 kinase binding domain using MOE software.

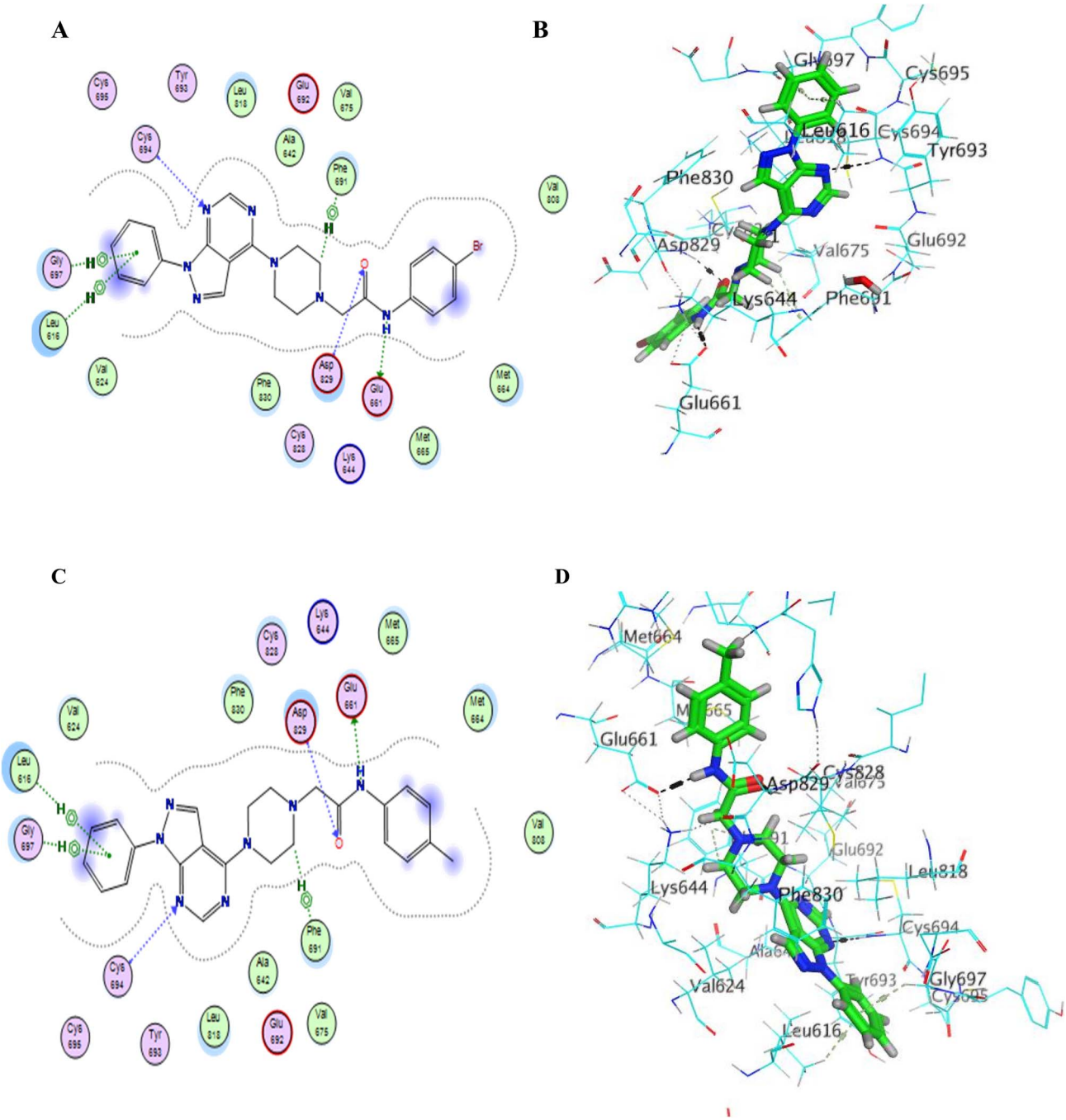

Fig. 6 (A–D) 2D & 3D representation of compounds **XIIb** (A and B) & **XIIe** (C and D) in FLT3 kinase binding domain (PDB code: 4RT7), they established the same key interactions as the lead compound (quizartinib); N_2 pyrimidine form one hydrogen bond with Cys 694 residue; NH of amide linker makes a hydrogen bond with Glu661; C═O of amide moiety makes a hydrogen bond with Asp 829.

the antiproliferative activity of these compounds so molecular dynamics was performed to gain more insight into the binding mode of these compounds and the results revealed that the low lifetime of hydrogen bond affect hydrogen bond stability with the essential amino acids.

In silico ADME study was conducted and predicted these molecules to exhibit good oral bioavailability and that they can pass BBB so they may be good candidates for brain tumors. Finally and according to the *in vitro* and *in silico* studies, these compounds have a significant antiproliferative activity but their mechanism of action will be a subject under investigation in our future work.

Experimental

Chemistry

Starting materials, reagents and solvents were purchased from Sigma Aldrich, Loba Chem and Al Gomhouria and were used

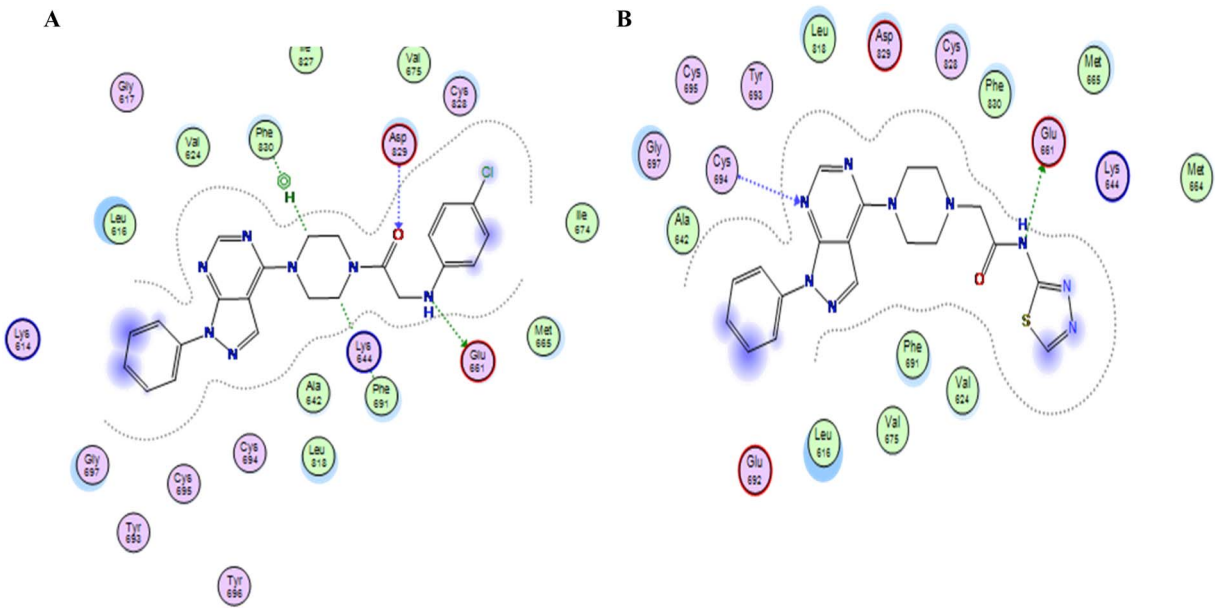

Fig. 7 (A & B) 2D representation of compound **XVIIIc** & **XVI** in FLT3 kinase binding domain respectively (PDB code: 4RT7), missing one key interaction.

Table 4 Percent inhibition at 10 μM against FLT3 enzymatic activity achieved by the designed compounds

No.	CPD ID	FLT3% inhibition
1	**XIIa**	26
2	**XIIb**	15
3	**XIIc**	15
4	**XIId**	24
5	**XIIe**	16
6	**XIIf**	14
7	**XIII**	9
8	**XIV**	18
9	**XV**	5
10	**XVI**	29
11	**XVIIIa**	20
12	**XVIIIb**	10
13	**XVIIIc**	8
14	**XVIIId**	9
15	**XVIIIe**	13
16	**XXIa**	11
17	**XXIb**	9
18	**XXIc**	5
19	**XXId**	8
20	**XXIe**	6
21	**XXIf**	5

without further purification. Benzoyl chloride and its derivatives were purchased from Alfa Aesar Pharmaceuticals and were used without further purification. All the reactions were monitored and the purity of the compounds was checked by ascending thin layer chromatography (TLC) on silica gel-coated aluminum plates (Merck 60 F254, 0.25 mm) using mixture of DCM and methanol (9 : 1) and the spots were seen under ultra violet light at 254 and 366 nm. Melting points were calculated without correction in open capillaries using Stuart (Biocote) scientific melting point apparatus.

^{1}H NMR spectra were recorded in δ scale given in ppm on a Bruker 400 MHz spectrophotometer and referred to TMS at Drug Discovery Center at Faculty of Pharmacy, Ain-Shams University. Whereas ^{13}C NMR spectra were recorded at 100 MHz. FT-IR spectra were determined (KBr) using Shimadzu infrared spectrometer (IR-435) and FT-IR 1650 (PerkinElmer), Faculty of Pharmacy, MSA University. EI-MS spectra were recorded on Finnigan Mat SSQ 7000 (70 eV) mass spectrometer at Regional Center for Mycology and Biotechnology at El Azhar University. Elemental analyses were performed at Regional Center for Mycology and Biotechnology at El-Azhar University. High resolution mass spectra have been recorded on QTOF Firmware Version 26.723 at Natural Products Research Lab at Faculty of Pharmacy, Fayoum University. Starting intermediates in Scheme 1 was prepared according to the reported procedures.

General procedure for the preparation of compound XIIa–f

To a solution of compound **XI** (0.28 g, 1 mmol) in DMF (20 mL), sodium bicarbonate (0.08 g, 1 mmol) and potassium iodide (0.16 g, 1 mmol) were added. 2-Chloro-*N*-substituted phenyl acetamide derivatives **IIa–f** (1 mol) was added to the previous reaction mixture and stirred at room temperature for 36 hours. The reaction mixture was added on to ice cold water to afford a precipitate which was filtered and left to dry. The resulting solid was recrystallized from absolute ethanol to give the titled compounds **XIIa–f**.

***n*-Phenyl-2-(4-(1-phenyl-1*H*-pyrazolo[3,4-*d*]pyrimidin-4-yl) piperazin-1-yl)acetamide XIIa.** The titled compound was separated as brown solid 0.27 g (yield = 70%); mp 180–182 °C; ^{1}H NMR (DMSO-d_6, 400 MHz) δ (ppm): 9.83 (s, 1H, NH, D_2O exchangeable), 8.62 (s, 1H, CH pyrimidine), 8.39 (s, 1H, CH

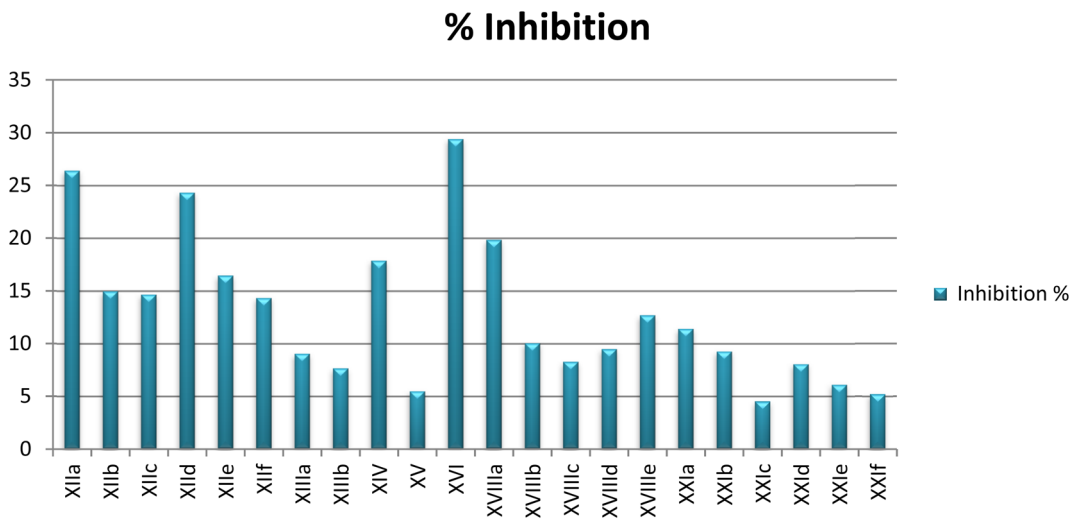

Fig. 8 Percent inhibition at 10 μM against FLT3 enzymatic activity achieved by designed compounds.

pyrazole), 8.18 (d, J = 8, 2H, ArH), 7.68 (d, J = 10.4, 2H, ArH), 7.56 (t, J = 8.8, 8.8, 2H, ArH), 7.37 (t, J = 6.4, 12 1H, ArH), 7.32 (d, J = 8, 2H, ArH), 7.07 (t, J = 8.8, 8.8, 1H, ArH), 4.06 (broad s, 4H, piperazine), 3.25 (s, 2H, CH_2), 2.70 (broad s, 4H, piperazine); ^{13}C-NMR (DMSO-d_6, 100 MHz): δ (ppm): 168.8 C=O, 168.2, 157.0, 155.8, 154.4, 139.1, 136.5, 135.5, 132.8 2C, 129.5 2C, 126.8, 121.7 2C, 120.0 2C, 101.5, 61.7, 52.8 2C, 40.6 2C; FT-IR (υ max, cm^{-1}): 3316 (NH), 3034 (CH aromatic), 2948 (CH aliphatic), 1697 (C=O amide).

***n*-(4-Bromophenyl)-2-(4-(1-phenyl-1*H*-pyrazolo[3,4-*d*] pyrimidin-4-yl)piperazin-1-yl)acetamide XIIb.** The titled compound was separated as greyish white solid 0.40 g (yield = 82%); mp 146–147 °C; ^{1}H NMR (DMSO-d_6, 400 MHz) δ (ppm): 9.97 (s, 1H, NH, D_2O exchangeable), 8.61 (s, 1H, CH pyrimidine), 8.39 (s, 1H, CH pyrazole), 8.19 (d, J = 14.8, 2H, ArH), 7.66 (d, J = 10.4, 2H, ArH), 7.58 (d, J = 9.6, 2H, ArH), 7.51 (d, J = 9.6, 2H, ArH), 7.36 (t, J = 8.8, 10.4, 1H, ArH), 4.05 (broad s, 4H, piperazine), 3.25 (s, 2H, CH_2), 2.71 (broad s, 4H, piperazine); ^{13}C-NMR (DMSO-d_6, 100 MHz): δ (ppm): 168.9 C=O, 156.9, 155.8, 154.3, 139.0, 138.3, 135.4, 131.9 2C, 129.5 2C, 126.9, 122.0, 121.7 2C, 115.6 2C, 101.5, 61.7, 52.7 2C, 40.4 2C; FT-IR (υ max, cm^{-1}): 3298 (NH), 3047 (CH aromatic), 2819 (CH aliphatic), 1694 (C=O amide); MS: (M_w: 492.38), m/z: 492.59 (14.59%), 474.07 (100%); anal. calcd for $C_{23}H_{22}BrN_7O$, C 56.11, H 4.50, N 19.91 found C 56.38, H 4.72, N 20.04. HRMS (ESI) calcd for $C_{23}H_{22}BrN_7O$ [M + H]$^+$, 492.1069; found, 492.1132, [M + 2] 494.1111.

***n*-(4-Chlorophenyl)-2-(4-(1-phenyl-1*H*-pyrazolo[3,4-*d*] pyrimidin-4-yl)piperazin-1-yl)acetamide XIIc.** The titled compound was separated as yellowish white crystals 0.35 g (yield = 80%); mp 120–122 °C; ^{1}H NMR (DMSO-d_6, 400 MHz) δ (ppm): 9.99 (s, 1H, NH, D_2O exchangeable), 8.63 (s, 1H, CH pyrimidine), 8.40 (s, 1H, CH pyrazole), 8.19 (d, J = 14.8, 2H, ArH), 7.66 (d, J = 10.4 2H, ArH), 7.58 (d, J = 9.6 2H, ArH), 7.51 (d, J = 12.8, 2H, ArH), 7.36 (t, J = 8.8, 10.4, 1H, ArH), 4.05 (broad s, 4H, piperazine), 3.25 (s, 2H, CH_2), 2.73 (broad s, 4H,

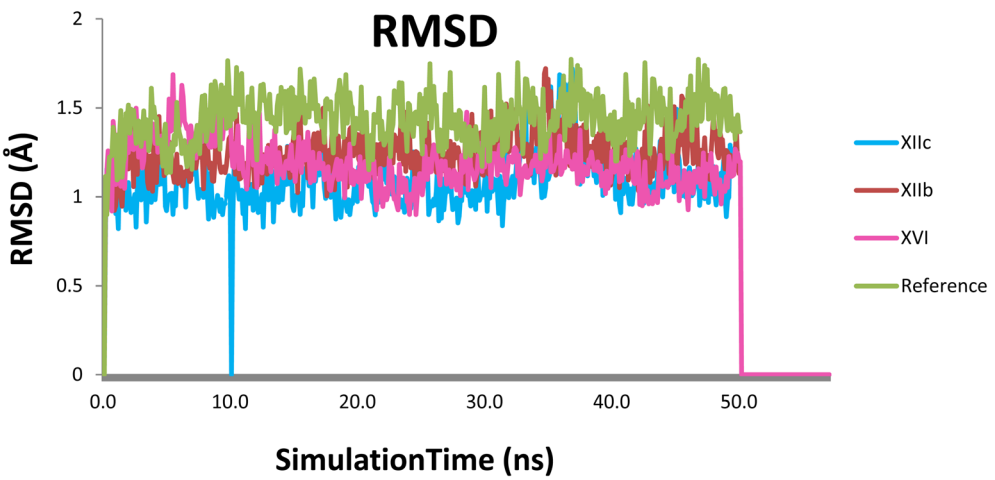

Fig. 9 RMSD plot of each compound with the protein, (**XIIb**: red, **XIIc**: blue, **XVI**: pink & reference: green).

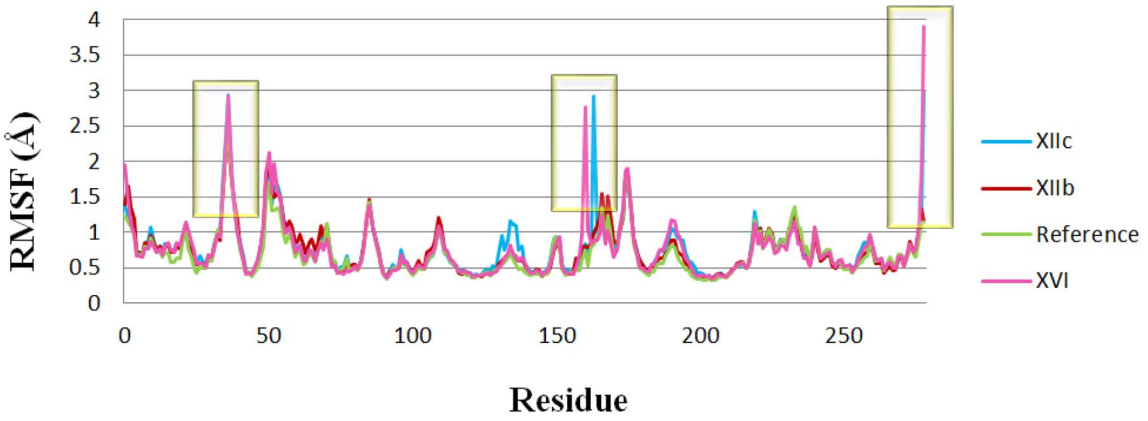

Fig. 10 RMSF for the protein residues in the 4 dynamic runs, (XIIb: red, XIIc: blue, XVI: pink & reference: green).

piperazine); ^{13}C-NMR (DMSO-d_6, 100 MHz): δ (ppm): 168.8 C=O, 156.9, 155.8, 154.3, 139.0, 138.3, 135.4, 131.9 2C, 129.5 2C, 126.9, 122.0 2C, 121.7 2C, 115.6, 101.5, 61.7, 52.7 2C, 40.4 2C; FT-IR (υ max, cm^{-1}): 3287 (NH), 3132 (CH aromatic), 2865 (CH aliphatic), 1649 (C=O amide); MS: (M_w: 447.93), m/z: 447.19 (7.02%), 329.00 (100%); anal. calcd for $C_{23}H_{22}ClN_7O$, C 61.67, H 4.95, N 21.89 found C 61.85, H 5.12, N 21.72.

***n*-(4-Methoxyphenyl)-2-(4-(1-phenyl-1*H*-pyrazolo[3,4-*d*] pyrimidin-4-yl)piperazin-1-yl)acetamide XIId.** The titled compound was separated as grey solid 0.33 g (yield = 75%); mp 156–158 °C; ^{1}H NMR (DMSO-d_6, 400 MHz) δ (ppm): 9.70 (s, 1H, NH, D_2O exchangeable), 8.62 (s, 1H, CH pyrimidine), 8.39 (s, 1H, CH pyrazole), 8.19 (d, J = 12, 2H, ArH), 7.58 (d, J = 8.4, 2H, ArH), 7.53 (m, 2H, ArH), 7.36 (t, J = 9.2, 11.2, 1H, ArH), 6.91 (d, J = 8.4, 2H, ArH), 4.07 (broad s, 4H, piperazine), 3.73 (s, 3H, OCH_3), 3.21 (s, 2H, CH_2), 2.71 (broad s, 4H, piperazine); ^{13}C-NMR (DMSO-d_6, 100 MHz): δ (ppm): 168.1 C=O, 157.0, 155.8, 154.4, 139.0, 135.5, 132.4, 129.6 2C, 127.0, 121.7 2C, 121.7 2C, 114.2 2C, 101.5, 64.9, 61.9, 55.6, 52.8 2C, 45.9 2C; FT-IR (υ max, cm^{-1}): 3326 (NH), 3134 (CH aromatic), 2922 (CH aliphatic), 1686 (C=O amide); MS: (M_w: 443.21), m/z: 443.83 (19.99%), 157.53 (100%); anal. calcd for $C_{24}H_{25}N_7O_2$, C 65.00, H 5.68, N 22.11 found C 64.93, H 5.86, N 21.97. HRMS (ESI) calcd for $C_{24}H_{25}N_7O_2$ [M + H]$^+$, 444.2070; found, 444.2144.

2-(4-(1-Phenyl-1*H*-pyrazolo[3,4-*d*]pyrimidin-4-yl)piperazin-1-yl)-*N*-(*p*-tolyl)acetamide XIIe. The titled compound was separated as yellow solid 0.25 g (yield 65%); mp 185–188 °C; ^{1}H NMR (DMSO-d_6, 400 MHz) δ (ppm): 9.75 (s, 1H, NH, D_2O exchangeable), 8.62 (s, 1H, CH pyrimidine), 8.39 (s, 1H, CH pyrazole), 8.18 (d, J = 7.6, 2H, ArH), 7.58 (d, J = 7.6, 2H, ArH), 7.54 (m, 2H, ArH), 7.36 (t, J = 8, 10, 1H, ArH), 7.14 (d, J = 9.6, 2H, ArH), 4.06 (broad s, 4H, piperazine), 3.23 (s, 2H, CH_2), 2.72 (broad s, 4H, piperazine), 2.26 (s, 3H, CH_3); ^{13}C-NMR (DMSO-d_6, 100 MHz): δ (ppm): 168.3, 157.01, 155.8, 154.4, 139.1, 136.5, 135.5, 132.8 2C, 129.5 2C, 126.8, 121.7 2C, 120.0 2C, 101.5, 61.8, 52.8 2C, 40.5 2C, 20.9; FT-IR (υ max, cm^{-1}): 3350 (NH), 3119 (CH aromatic), 2833 (CH aliphatic), 1692 (C=O amide); MS: (M_w: 427.51), m/z 427.62 (9.06%), 158.89 (100%); anal. calcd for $C_{24}H_{25}N_7O$, C 67.43, H 5.89, N 22.93 found C 67.59, H 6.11, N 23.16. HRMS (ESI) calcd for $C_{24}H_{25}N_7O$ [M + H]$^+$, 428.2121; found, 428.2229.

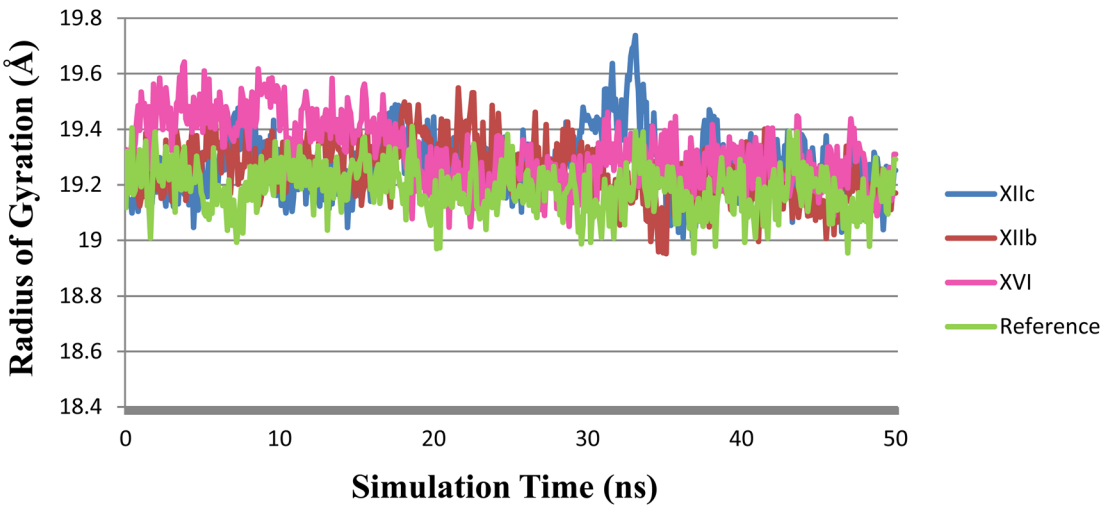

Fig. 11 R_g plot during the simulation time of 50 ns, (XIIb: red, XIIc: blue, XVI: pink & reference: green).

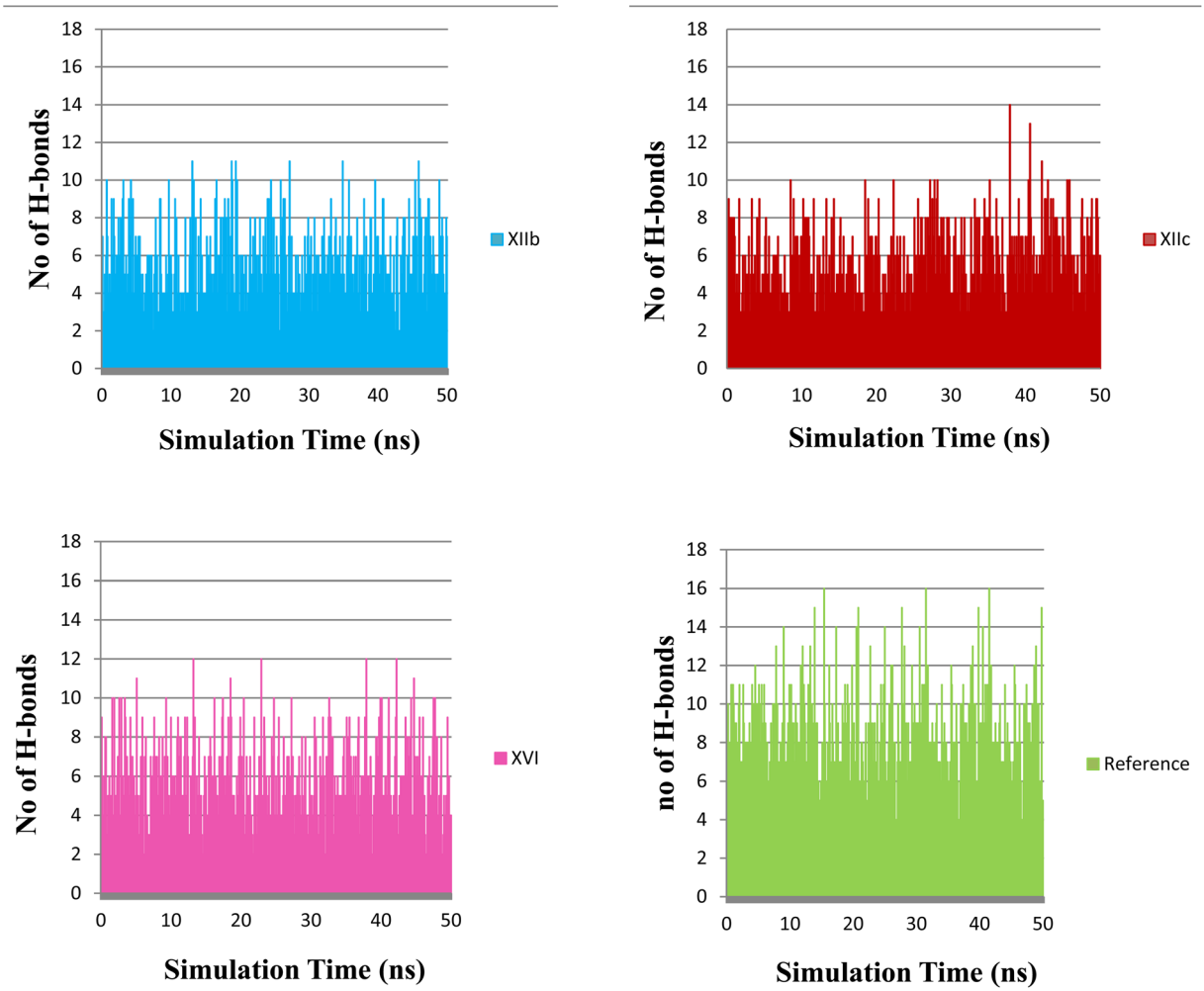

Fig. 12 The number of H-bonds formed between each compound and the protein, (**XIIb**: red, **XIIc**: blue, **XVI**: pink & reference: green).

Table 5 Hydrogen-bond analysis for the 50 ns of the respective MD trajectories, lifetime of H-bond means the percentage of snapshots in which the relevant hydrogen bond is formed. A dash indicates a low incidence of hydrogen bonds with a lifetime of less than 10%

Contributing amino acid	Lifetime of H-bond			
	XIIb	**XIIc**	**XVI**	Reference
Cys694	18.76%	—	—	89.31%
Glu661	40.81%	50.14%	33.75%	75.51%
Asp829	—	—	16.37%	81.95%

2-(4-(1-Phenyl-1*H*-pyrazolo[3,4-*d*]pyrimidin-4-yl)piperazin-1-yl)-*N*-(*m*-tolyl)acetamide XIIf. The titled compound was separated as creamy white solid 0.31 g (yield = 73%); mp 162–164 °C; ^{1}H NMR (DMSO-d_6, 400 MHz) δ (ppm): 9.74 (s, 1H, NH, D_2O exchangeable), 8.62 (s, 1H, CH pyrimidine), 8.39 (s, 1H, CH pyrazole), 8.19 (d, J = 9.2, 2H, ArH), 7.56 (t, J = 10.8, 7.2, 2H, ArH), 7.47 (m, 4H, ArH), 7.37 (t, J = 9.6, 6.4, 1H, ArH), 4.06 (broad s, 4H, piperazine), 3.23 (s, 2H, CH_2), 2.73 (broad s, 4H, piperazine), 2.69 (s, 3H, CH_3); ^{13}C-NMR (DMSO-d_6, 100 MHz): δ (ppm): 168.8, 168.2, 156.9, 155.8, 154.3, 139.1, 136.5, 135.5, 132.8 2C, 129.5 2C, 129.5, 126.8, 121.7, 120.0, 115.6, 101.5, 61.7, 52.8 2C, 40.4 2C, 20.9; FT-IR (υ max, cm^{-1}): 3253 (NH), 3053 (CH aromatic), 2933 (CH aliphatic), 1665 (C=O amide); MS: (M_w: 428.51), m/z: 428.27 (37.36%), 204.61 (100%); anal. calcd for $C_{24}H_{25}N_7O$, C 67.43, H 5.89, N 22.93 found C 67.54, H 6.13, N 22.75.

General procedure for preparation of XIII & XIV

To a solution of compound **XI** (0.28 g, 1 mmol) in DMF (20 mL), sodium bicarbonate (0.08 g, 1 mmol) and potassium iodide (0.16 g, 1 mmol) were added. Naphthyl chloroacetate derivatives **IIa**,**b** (1 mmol) or phenyl chloroacetate **IV** (0.17 g, 1 mmol) were added to the previous reaction mixture and stirred at room temperature for 24 hours. The reaction mixture was added on to water (30 mL) to afford a precipitate which was filtered and left to dry. The resulting solid was recrystallized from ethyl acetate/*n*-hexane (3 : 1) to give the titled compounds.

Naphthalen-1-yl 2-(4-(1-phenyl-1*H*-pyrazolo [3,4-*d*]pyrimidin-4-yl)piperazin-1-yl)acetate XIII. The titled compound was separated as greyish white solid 0.25 g (yield = 55%); mp 137–139 °C

Table 6 Computer-aided ADMET screening results of the synthesized compounds

CPD ID	BBB-Lev[a]	Absorp-lev[b]	Sol-lev[c]	Hepatotox[d]	Hepatox prob	CYP2D6[e]	*A* log *P*98	PSA-2D[f]
XIIa	2	0	2	0	0.231	1	2.832	75.947
XIIb	2	0	2	0	0.172	1	3.318	75.947
XIIc	2	0	2	0	0.278	1	3.496	75.947
XIId	3	0	2	0	0.258	1	2.815	84.877
XIIe	2	0	2	0	0.251	1	3.58	75.947
XIIf	2	0	2	0	0.192	1	3.318	75.947
XIII	1	0	2	0	0.298	1	4.387	72.067
XIV	2	0	2	0	0.205	1	3.479	72.067
XV	1	0	2	0	0.337	1	3.926	58.646
XVI	4	0	2	0	0.403	0	4.361	98.469
XVIIIa	2	0	2	0	0.225	1	2.779	75.947
XVIIIb	2	0	2	0	0.152	0	3.266	75.947
XVIIIc	2	0	2	0	0.271	0	3.444	75.947
XVIIId	3	0	2	0	0.258	1	2.763	84.877
XVIIIe	2	0	2	0	0.258	1	3.528	75.947
XXIa	2	0	2	0	0.218	0	3.798	75.947
XXIb	1	0	2	0	0.245	1	4.463	75.947
XXIc	2	0	2	0	0.225	0	3.782	84.877
XXId	2	0	2	0	0.192	1	4.284	75.947
XXIe	1	0	1	0	0.218	0	4.547	75.947
XXIf	2	0	2	0	0.218	0	3.926	75.947

[a] BBB_level; 4 = undefined, 2 = medium penetration, 1 = high penetration. [b] Absorp_level; 3 = very low absorption, 2 = low absorption, 1 = moderate absorption, 0 = good absorption. [c] SOl LEV; 2 = low solubility, 1 = very low but soluble, 0 = extremely low solubility. [d] Hepatotox_level; 1 = toxic, 0 = non-toxic. [e] CYP 2D6; 1 = likely to inhibit, 0 = non-inhibitor. [f] PSA (polar surface area); cpds must have log *P* value not greater than 5.0 to attain a reasonable probability of being well absorbed.

^{1}H NMR (DMSO-d_6, 400 MHz) δ (ppm): 8.64 (s, 1H, ArH, CH pyrimidine), 8.41 (s, 1H, ArH, CH pyrazole), 8.19 (d, J = 9.2, 2H, ArH), 7.94 (m, 3H, ArH), 7.73 (m, 2H, ArH), 7.57 (m, 3H, ArH), 7.52 (m, 2H, ArH), 4.76 (s, 2H, CH_2), 4.07 (broad s, 4H, piperazine), 2.85 (broad s, 4H, piperazine); ^{13}C-NMR (DMSO-d_6, 100 MHz): δ (ppm): 168.8 C=O, 163.1, 157.0, 155.8, 154.4, 139.1, 136.5, 135.5, 132.8, 129.5 2C, 129.5 2C, 126.8 2C, 121.7 2C, 120.0 2C, 115.6, 114.2, 101.5, 61.7, 52.8 2C, 40.6 2C; FT-IR (υ max, cm^{-1}): 3042 (CH aromatic), 2873 (CH aliphatic), 1735 (C=O ester); MS: (M_w: 465.53), m/z 465.46 (15.70%), 220.24 (100%); anal. calcd for $C_{27}H_{24}N_6O_2$, C 69.81, H 5.21, N 18.09 found C 70.04, H 5.39, N 18.35.

Phenyl 2-(4-(1-phenyl-1*H*-pyrazolo[3,4-*d*]pyrimidin-4-yl) piperazin-1-yl)acetate XIV. The titled compound was separated as a yellow solid 0.20 g (yield = 50%); mp 152–154 °C; FT-^{1}H NMR (DMSO-d_6, 400 MHz) δ (ppm): 8.56 (s, 1H, CH pyrimidine), 8.36 (s, 1H, CH pyrazole), 8.12 (d, J = 8, 2H, ArH), 7.68 (d, J = 12, 2H, ArH), 7.54 (t, J = 8, 8, 2H, ArH), 7.33 (M, 3H, ArH), 7.07 (t, J =

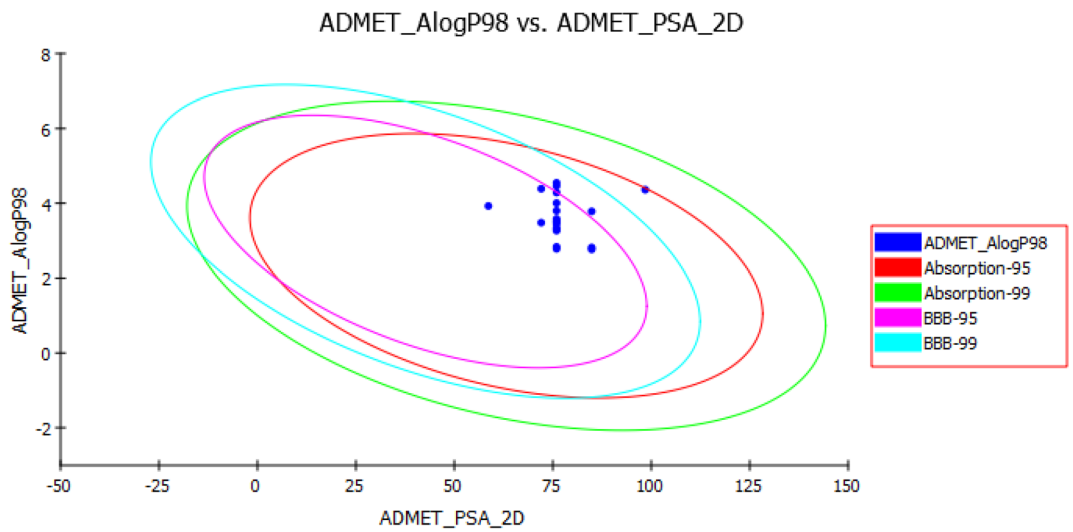

Fig. 13 Human intestinal absorption (HIA) and blood–brain barrier plot for the newly synthesized compounds.

8, 8, 1H, ArH) 4.03 (t, 4H, piperazine), 3.23 (s, 2H, CH_2), 2.70 (broad s, 4H, piperazine); ^{13}C-NMR (DMSO-d_6, 100 MHz): δ (ppm): 168.2 C=O, 155.8, 154.4, 139.1, 136.5, 135.5, 132.8 2C, 129.5 2C, 129.5 2C, 126.8, 121.7 2C, 120.0, 101.5, 62.7, 52.8 2C, 40.6 2C IR (υ max, cm^{-1}): 3122 (CH aromatic), 2940 (CH aliphatic), 1759 (C=O ester); MS: (M_w: 414.06), m/z: 414.06 (44.9%), 114.43 (100%); anal. calcd for $C_{23}H_{22}N_6O_2$ (M_w: 414.47), C 66.65, H 5.35, N 20.28 found C 66.73, H 5.19, N 20.37.

***n*-Phenyl-4-(1-phenyl-1*H*-pyrazolo[3,4-*d*]pyrimidin-4-yl) piperazine-1-carbothioamide XV.** To a solution of compound **XI** (0.28 g, 1 mmol) in dry DCM (5 mL), phenyl iso-thiocynate (0.13 g, 0.12 mL, 1 mmol) was added and the reaction mixture was refluxed for 2 hours to afford a precipitate which was filtered on hot and left to dry. The resulting solid was recrystallized from ethanol to give the titled compound **XV**.

The titled compound was separated as a white solid 0.31 g (yield = 75%); mp 175–177 °C; ^{1}H NMR (DMSO-d_6, 400 MHz) δ (ppm): 9.38 (s, 1H, NH, D_2O exchangeable), 8.66 (s, 1H, CH pyrimidine), 8.46 (s, 1H, CH pyrazole), 8.18 (d, J = 8, 2H, ArH), 7.57 (t, J = 8, 4, 2H, ArH), 7.39 (t, J = 8, 8, 2H, ArH), 7.37 (m, 4H, ArH), 4.13 (broad s, 4H, piperazine), 3.29 (broad s, 4H, piperazine); ^{13}C-NMR (DMSO-d_6, 100 MHz): δ (ppm): 170.3 (C=S), 163.1, 157.0, 155.8, 145.3, 138.9, 135.8, 135.4, 130.3, 129.6 2C, 128.9 2C, 127.6, 127.1, 121.8 2C, 101.6, 55.6 2C, 40.1 2C; FT-IR (υ max, cm^{-1}): 3474 (NH), 3238 (CH aromatic), 2928 (CH aliphatic); MS: (M_w: 415.52): m/z 415.96 (32.49%), 416.80 (24.82%), 84.87 (100%); anal. calcd for $C_{22}H_{21}N_7S$, C 63.59, H 5.09, N 23.60 found C 63.45, H 5.17, N 23.84.

2-(4-(1-Phenyl-1*H*-pyrazolo[3,4-*d*]pyrimidin-4-yl)piperazin-1-yl)-*N*-(1,3,4-thiadiazol-2-yl)acetamide XVI. To a solution of compound **XI** (0.28 g, 1 mmol) in DMF (20 mL), sodium bicarbonate (0.08 g, 1 mmol) and potassium iodide (0.16 g, 1 mmol) were added. 2-Chloro-*N*-(1,3,4-thiadiazol-2-yl)acetamide **V** (0.17 g, 1 mmol) was added to the previous reaction mixture and stirred at room temperature for 36 hours. The reaction mixture was added on to ice cold water to afford a precipitate which was filtered and left to dry. The resulting solid was recrystallized from absolute ethanol to give the titled compound **XVI**.

The titled compound was separated as buff crystals 0.13 g (yield = 75%); mp 190–192 °C; ^{1}H NMR (DMSO-d_6, 400 MHz) δ (ppm): 9.44 (s, 1H, NH, D_2O exchangeable), 9.43 (s, 1H, ArH), 8.66 (s, 1H, CH pyrimidine), 8.46 (s, 1H, CH pyrazole), 8.18 (d, J = 8, 2H, ArH), 7.57 (t, J = 8, 8, 2H, ArH), 7.38 (t, J = 4, 4, 1H, ArH), 4.21 (t, J = 4, 4, 4H, piperazine), 3.28 (t, J = 4, 4, 4H, piperazine), 2.72 (s, 2H, CH_2); ^{13}C-NMR (DMSO-d_6, 100 MHz): δ (ppm): 168.9 C=O, 156.9, 155.8, 139.0, 138.3, 135.4, 131.9, 129.5 2C, 126.9, 122.0, 121.7 2C, 101.5, 61.7, 52.7 2C, 40.2 2C; FT-IR (υ max, cm^{-1}): 3404 (NH), 3113 (CH aromatic), 2918 (CH aliphatic), 1690 (C=O amide); MS: (M_w: 421.14), m/z: 421.46 (47.71%), 57.12 (100%); anal. calcd for $C_{19}H_{19}N_9OS$ (M_w: 421.48), C 54.14, H 4.54, N 29.91 found C 54.31, H 4.68, N 30.15.

2-Chloro-1-(4-(1-phenyl-1*H*-pyrazolo[3,4-*d*]pyrimidin-4-yl) piperazin-1-yl)ethan-1-one XVII. To a solution of compound **XI** (0.28 g, 1 mmol) in DMF (10 mL), anhydrous sodium acetate (0.08 g, 1 mmol) was added. 2-Chloroacetyl chloride **I** (0.11 g, 0.07 mL, 1 mmol) was then added drop wise to the reaction mixture and refluxed for 16 hours. The reaction mixture was poured onto ice, filtered and used immediately.

General procedure for preparation of compound XVIIIa–f

To a solution of compound **XVII** (0.35 g, 1 mmol) in DMF (25 mL), sodium bicarbonate (0.08 g, 1 mmol) and potassium iodide (0.16 g, 1 mmol) were added. Aromatic amine derivatives (1 mmol) were added to the previous reaction mixture and stirred at room temperature for 48 hours. The reaction mixture was added on to ice cold water to afford a precipitate which was filtered and left to dry. The resulting solid was recrystallized from absolute ethanol to give the titled compounds **XVIIIa–f**.

1-(4-(1-Phenyl-1*H*-pyrazolo[3,4-*d*]pyrimidin-4-yl)piperazin-1-yl)-2-(phenylamino)ethan-1-one XVIIIa. The titled compound was separated as buff solid 0.25 g (yield = 62%); mp 180–182 °C; ^{1}H NMR (DMSO-d_6, 400 MHz) δ (ppm): 8.62 (s, 1H, CH pyrimidine), 8.39 (s, 1H, CH pyrazole), 8.18 (d, J = 8, 2H, ArH), 7.65 (d, J = 12, 2H, ArH), 7.58 (t, J = 8, 8, 2H, ArH), 7.38 (t, J = 8, 8, 1H, ArH), 7.30 (d, J = 8, 2H, ArH), 7.09 (t, J = 8, 8, 1H, ArH), 5.51 (s, 1H, NH, D_2O exchangeable), 4.08 (broad s, 4H, piperazine), 3.76 (broad s, 4H, piperazine) 3.25 (s, 2H, CH_2); ^{13}C-NMR (DMSO-d_6, 100 MHz): δ (ppm): 168.8, 163.1, 155.8, 154.4, 139.1, 136.5, 135.5, 132.8, 129.5 (2C), 129.5 2C, 126.8, 121.7, 120.0 2C, 115.6 2C, 101.5, 52.8, 40.6 2C, 40.4 2C; FT-IR (υ max, cm^{-1}): 3316 (NH), 3034 (CH aromatic), 2948 (CH aliphatic), 1697 (C=O amide); anal. calcd for $C_{23}H_{23}N_7O$ (M_w: 413.49), C 66.81, H 5.61, N 23.71 found C 66.9, H 5.71, N 23.94.

2-((4-Bromophenyl)amino)-1-(4-(1-phenyl-1*H*-pyrazolo[3,4-*d*] pyrimidin-4-yl)piperazin-1-yl)ethan-1-one XVIIIb. The titled compound was separated as greyish white solid 0.2 g (yield = 80%); mp 146–147 °C; ^{1}H NMR (DMSO-d_6, 400 MHz) δ (ppm): 8.59 (s, 1H, CH pyrimidine), 8.43 (s, 1H, CH pyrazole), 8.20 (d, J = 12, 2H, ArH), 7.56 (t, J = 8, 8, 2H, ArH), 7.37 (t, J = 8, 4, 1H, ArH), 7.23 (d, J = 8, 2H, ArH), 6.66 (d, J = 12, 2H, ArH), 5.90 (s, 1H, NH, D_2O exchangeable), 4.04 (m, 8H, piperazine), 3.98 (s, 2H, CH_2); ^{13}C-NMR (DMSO-d_6, 100 MHz): δ (ppm): 164.2, 157.0, 155.8, 139.9, 139.3, 135.5, 129.5 2C, 129.4, 129.0 2C, 127.7, 126.8, 121.7 2C, 121.6 2C, 102.2, 52.8, 40.6 2C, 40.2 2C; FT-IR (υ max, cm^{-1}): 3298 (NH), 3047 (CH aromatic), 2819 (CH aliphatic), 1694 (C=O amide); MS: (M_w: 492.38), m/z 492.35 (29.68%). 436.13 (100%); anal. calcd for $C_{23}H_{22}BrN_7O$ (M_w: 492.38), C 56.11, H 4.50, N 19.91 found C 56.34, H 4.73, N 20.15. HRMS (ESI) calcd for $C_{23}H_{22}BrN_7O$ $[M + H]^+$ 492.1069; found, 492.1129, [M + 2] 494.1114.

2-((4-Chlorophenyl)amino)-1-(4-(1-phenyl-1*H*-pyrazolo[3,4-*d*] pyrimidin-4-yl)piperazin-1-yl)ethan-1-one XVIIIc. The titled compound was separated as yellowish white crystals 0.2 g (yield = 80%); mp 146–147 °C; ^{1}H NMR (DMSO-d_6, 400 MHz) δ (ppm): 8.58 (s, 1H, CH pyrimidine), 8.46 (s, 1H, CH pyrazole), 8.19 (d, J = 8, 2H, ArH), 7.57 (t, J = 8,8, 2H, ArH), 7.37 (t, J = 8, 8, 1H, ArH), 7.11 (d, J = 8, 2H, ArH), 6.70 (d, J = 12, 2H, ArH), 5.87 (s, 1H, NH D_2O exchangeable), 4.05 (m, 8H, piperazine), 3.59 (s, 2H, CH_2); ^{13}C-NMR (DMSO-d_6, 100 MHz): δ (ppm): 168.9, 163.1, 156.9, 154.3, 139.0, 138.3, 135.4, 131.9, 129.5 2C, 126.9 2C, 122.0, 121.7 2C, 115.6 2C, 101.5, 52.7, 40.4 2C, 40.2 2C; FT-IR (υ max, cm^{-1}): 3287 (NH), 3132 (CH aromatic), 2865 (CH aliphatic), 1649 (C=O

amide); MS: (M_w: 447.93) m/z 447.08, (40.52%), 103.30 (100%); anal. calcd for $C_{23}H_{22}ClN_7O$ (M_w: 447.93), C 61.67, H 4.95, N 21.89 found C 61.88, H 5.11, N 21.75. HRMS (ESI) calcd for $C_{23}H_{22}ClN_7O$ $[M + H]^+$ 448.1574; found, 448.1651, [M + 2] 450.1630.

2-((4-Methoxyphenyl)amino)-1-(4-(1-phenyl-1*H*-pyrazolo[3,4-*d*]pyrimidin-4-yl)piperazin-1-yl)ethan-1-one XVIIId. The titled compound was separated as grey solid 0.2 g (yield = 80%); mp 146–147 °C; ^{1}H NMR (DMSO-d_6, 400 MHz) δ (ppm): 8.62 (s, 1H, CH pyrimidine), 8.39 (s, 1H, CH pyrazole), 8.19 (d, J = 12, 2H, ArH), 7.58 (m, 4H, ArH), 7.39 (t, J = 12, 12, 1H, ArH), 6.91 (d, J = 8, 2H, ArH), 5.40 (s, 1H, NH, D_2O exchangeable), 4.07 (broad s, 4H, piperazine), 4.05 (broad s, 4H, piperazine), 3.73 (s, 3H, OCH_3), 3.21 (s, 2H, CH_2); ^{13}C-NMR (DMSO-d_6, 100 MHz): δ (ppm): 168.1, 163.1, 157.0, 155.8, 154.4, 139.0, 135.5, 132.4 2C, 129.6 2C, 127.0, 121.7 2C, 115.6 2C, 114.2 2C, 101.5, 55.6, 52.8, 45.9 2C, 40.4 2C; FT-IR (υ max, cm^{-1}): 3326 (NH), 3134 (CH aromatic), 2922 (CH aliphatic), 1686 (C=O amide); MS: (M_w: 443.51), m/z 443.39 (35.91%), 160.18 (100%); anal. calcd for $C_{24}H_{25}N_7O_2$ (M_w: 443.51), C 65.00, H 5.68, N 22.11 found C 64.79, H 5.79, N 21.98.

1-(4-(1-Phenyl-1*H*-pyrazolo[3,4-*d*]pyrimidin-4-yl)piperazin-1-yl)-2-(*p*-tolylamino)ethan-1-one XVIIIe. The titled compound was separated as faint yellow solid 0.15 g (yield = 65%); mp 187 °C; ^{1}H NMR (DMSO-d_6, 400 MHz) δ (ppm): 8.58 (s, 1H, CH pyrimidine), 8.42 (s, 1H, CH pyrazole), 8.19 (d, J = 4, 2H, ArH), 7.57 (t, J = 8, 12, 2H, ArH), 7.37 (t, J = 8, 8, 1H, ArH), 6.92 (d, J = 8, 2H, ArH), 6.60 (d, J = 16, 2H, ArH), 5.38 (s, 1H, NH, D_2O exchangeable), 4.03 (m, 8H, piperazine), 3.76 (s, 3H, CH_3), 2.15 (s, 2H, CH_2); ^{13}C-NMR (DMSO-d_6, 100 MHz): δ (ppm): 168.3, 157.0, 155.8, 154.4, 139.1, 136.5, 135.5, 132.8, 129.5 2C, 129.5 2C, 126.8, 121.7 2C, 120.0 2C, 101.5, 61.8, 52.8 2C, 40.5 2C, 20.9; FT-IR (υ max, cm^{-1}): 3350 (NH), 3119 (CH aromatic), 2833 (CH aliphatic), 1692 (C=O amide); MS: (M_w: 427.51): m/z 427.15 (30.83%), 69.12 (100%); anal. calcd for $C_{24}H_{25}N_7O$ (M_w: 427.51), C 67.43, H 5.89, N 22.93 found C 67.59, H 6.05, N 23.78.

Aroyl isothiocyanate XXa–f

To a solution of ammonium thiocyanate (0.07 g, 1 mmol) in dry acetone (30 mL), the appropriate freshly prepared aroyl chloride derivatives (1 mmol) were added dropwise with stirring. The reaction mixture was continuously stirred vigorously for 45 minutes. The reaction was monitored by TLC until a new spot of intermediate **XXa–f** is formed and used directly in the following step.

General procedure for the preparation of compound XXIa–f

The solution resulted from the previous reaction **XXa–f** was added to a solution of intermediate **XI** (0.28 g, 1 mmol) in dry acetone (15 mL) and stirred for 36 hours at room temperature until a precipitate is formed. The formed precipitate was washed with cold water to yield our target compounds **XXIa–f**.

***N*-(4-(1-Phenyl-1*H*-pyrazolo[3,4-*d*]pyrimidin-4-yl)piperazine-1-carbonothioyl)benzamide XXIa.** The titled compound was separated as creamy white solid 0.03 g (yield = 80%); mp 146–147 °C; ^{1}H NMR (DMSO-d_6, 400 MHz) δ (ppm): 11.09 (s, 1H, NH, D_2O exchangeable), 8.55 (s, 1H, CH pyrimidine), 8.43 (s, 1H, CH pyrazole), 8.19 (d, J = 8.4, 2H, ArH), 7.93 (d, J = 8.4, 2H, ArH), 7.74 (t, J = 8.8, 10, 2H, ArH), 7.56 (t, J = 8, 8, 1H, ArH), 7.53 (m, 2H, ArH), 7.37 (t, J = 9.6, 7.6, 1H, ArH), 4.04 (broad s, 4H, piperazine), 3.73 (broad s, 4H, piperazine); ^{13}C-NMR (DMSO-d_6, 100 MHz): δ (ppm):170.3, 168.1, 163.1, 157.0, 155.8, 154.4, 145.3, 138.9, 135.8, 135.4, 130.3, 129.6 2C, 128.9 2C, 127.6, 127.1, 121.8 2C, 101.6, 55.6 2C, 40.1 2C; FT-IR (υ max, cm^{-1}): 3400 (NH), 3082 (CH aromatic), 2925(CH aliphatic), 1572 (C=O amide); MS: (M_w: 443.53), m/z 443.54 (40.18%), 77.91 (100%); anal. calcd for $C_{23}H_{21}N_7OS$, C 62.29, H 4.77, N 22.11 found C 62.41, H 4.89, N 21.97.

4-Fluoro-*N*-(4-(1-phenyl-1*H*-pyrazolo[3,4-*d*]pyrimidin-4-yl) piperazine-1-carbonothioyl)benzamide XXIb. The titled compound was separated as a white solid 0.39 g (yield = 85%); mp 180–182 °C; ^{1}H NMR (DMSO-d_6, 400 MHz) δ (ppm): 11.12 (s, 1H, NH, D_2O exchangeable), 8.55 (s, 1H, CH pyrimidine), 8.43 (s, 1H, CH pyrazole), 8.18 (d, J = 6.8, 2H, ArH), 8.07 (d, J = 8, 2H, ArH), 8.05 (d, J = 8, 2H, ArH), 7.56 (t, J = 8, 8, 8, 2H, ArH), 7.38 (m, 2H, ArH), 4.12 (m, 8H, piperazine); FT-IR (υ max, cm^{-1}): 3416 (NH), 3069 (CH aromatic), 2940 (CH aliphatic), 1650 (C=O amide); anal. calcd for: $C_{23}H_{20}FN_7OS$, C 59.86, H 4.37, N 21.24 found C 60.04, H 4.46, N 21.45. HRMS (ESI) calcd for $C_{23}H_{20}FN_7OS$ $[M + H]^+$ 462.1434; found, 462.1500.

4-Bromo-*N*-(4-(1-phenyl-1*H*-pyrazolo[3,4-*d*]pyrimidin-4-yl) piperazine-1-carbonothioyl)benzamide XXIc. The titled compound was separated as creamy white solid 0.47 g (yield = 90%); mp 182–184 °C; ^{1}H NMR (DMSO-d_6, 400 MHz) δ (ppm): 11.09 (s, 1H, NH, D_2O exchangeable), 8.55 (s, 1H, CH pyrimidine), 8.43 (s, 1H, CH pyrazole), 8.19 (d, J = 8, 2H, ArH), 7.91 (d, J = 8, 2H, ArH), 7.74 (d, J = 12, 2H, ArH), 7.56 (t, J = 8, 8, 2H, ArH), 7.37 (t, J = 8, 8, 1H, ArH), 4.26 (m, 8H, piperazine); FT-IR (υ max, cm^{-1}): 3232 (NH), 3052 (CH aromatic), 2920 (CH aliphatic), 1673 (C=O amide); MS: (M_w: 522.47), m/z 522.47 (22.33), 310.23 (100%): anal. calcd for: $C_{23}H_{20}BrN_7OS$, C 52.88, H 3.86, N 18.77 found C 52.67, H 3.98, N 19.03. HRMS (ESI) calcd for $C_{23}H_{20}BrN_7OS$ $[M + H]^+$ 522.0633; found, 522.0747, [M + 2] 524.0728.

4-Chloro-*N*-(4-(1-phenyl-1*H*-pyrazolo[3,4-*d*]pyrimidin-4-yl) piperazine-1-carbonothioyl)benzamide XXId. The titled compound was separated as white solid 0.04 g (yield = 85%); mp 136–137 °C; ^{1}H NMR (DMSO-d_6, 400 MHz) δ (ppm): 11.12 (s, 1H, NH, D_2O exchangeable), 8.56 (s, 1H, CH pyrimidine), 8.43 (s, 1H, CH pyrazole), 8.17 (d, J = 8, 2H, ArH), 7.98 (d, J = 8, 2H, ArH), 7.56 (t, J = 12, 4, 2H, ArH), 7.37 (t, J = 8, 8, 1H, ArH), 7.07 (d, J = 12, 2H, ArH), 4.06 (broad s, 4H, piperazine), 3.73 (broad s, 4H, piperazine); ^{13}C-NMR (DMSO-d_6, 100 MHz): δ (ppm): 170.3, 163.1, 157.0, 155.8, 145.3, 138.9, 135.8, 135.4, 130.3, 129.6 2C, 128.9 2C, 127.6, 127.1, 121.8 2C, 115.6, 101.6, 55.6 2C, 40.1 2C; FT-IR (υ max, cm^{-1}): 3280 (NH), 3114 (CH aromatic), 2830 (CH aliphatic), 1634 (C=O amide); MS: (M_w: 477.11), m/z 477.14 (69.88%), 446.49 (100%): anal. calcd for $C_{23}H_{20}ClN_7OS$, C 57.80, H 4.22, N 20.51 found C 58.04, H 4.36, N 20.78. HRMS (ESI) calcd for $C_{23}H_{20}ClN_7OS$ $[M + H]^+$ 478.1139; found, 478.1204, [M + 2] 480.1184.

4-Methoxy-*N*-(4-(1-phenyl-1*H*-pyrazolo[3,4-*d*]pyrimidin-4-yl) piperazine-1-carbonothioyl)benzamide XXIe. The titled

compound was separated as white solid 0.35 g (yield = 75%); mp 176–178 °C; ^{1}H NMR (DMSO-d_6, 400 MHz) δ (ppm): 10.80 (s, 1H, NH, D_2O exchangeable), 8.59 (s, 1H, CH pyrimidine), 8.43 (s, 1H, CH pyrazole), 8.18 (m, 2H, ArH), 7.89 (d, J = 8, 2H, ArH), 7.56 (t, J = 4, 12, 2H, ArH), 7.35 (m, 3H, ArH), 4.24 (m, 4H, piperazine), 3.60 (m, 4H, piperazine), 2.39 (s, 3H, OCH_3); ^{13}C-NMR (DMSO-d_6, 100 MHz): δ (ppm): 170.3, 168.1, 157.0, 155.8, 154.4, 139.0, 135.5, 132.4 2C, 129.6 2C, 127.0 2C, 121.7 2C, 121.7 2C, 114.2, 101.6, 61.9, 55.6 2C, 52.8 2C; FT-IR (υ max, cm^{-1}): 3401 (NH), 3089 (CH aromatic), 2949 (CH aliphatic), 1631 (C=O amide); MS: (M_w: 473.56), m/z 473.02 (14.52%), 318.12 (100%): anal. calcd for $C_{23}H_{20}ClN_7OS$, C 57.80, H 4.22, N 20.51 found C 58.04, H 4.36, N 20.78.

4-Methyl-*N*-(4-(1-phenyl-1*H*-pyrazolo[3,4-*d*]pyrimidin-4-yl) piperazine-1-carbonothioyl)benzamide XXIf. The titled compound was separated as white solid 0.29 g (yield = 65%); mp (168–170 °C); ^{1}H NMR (DMSO-d_6, 400 MHz) δ (ppm): 10.88 (s, 1H, NH, D_2O exchangeable), 8.55 (s, 1H, CH pyrimidine), 8.42 (s, 1H, CH pyrazole), 8.19 (d, J = 4, 2H, ArH), 7.99 (d, J = 8, 2H, ArH), 7.63 (d, J = 8, 2H, ArH), 7.56 (t, J = 8, 8, 2H, ArH), 7.37 (t, J = 8, 12, 1H, ArH), 4.26 (m, 8H, piperazine), 3.95 (s, 3H, CH_3); ^{13}C-NMR (DMSO-*d*6, 100 MHz): δ (ppm): 180.7, 163.6, 156.9, 155.8, 154.2, 139.1, 137.9, 135.6, 131.8, 130.8, 129.6 2C, 129.0 2C, 126.8 2C, 121.6 2C, 101.8, 52.8 2C, 40.6 2C, 21.5; FT-IR (υ max, cm^{-1}): 3443 (NH), 3116 (CH aromatic), 2870 (CH aliphatic), 1620 (C=O amide); MS: (M_w: 457.17), m/z 457.46 (31.83%), 420.55 (100%): anal. calcd for $C_{24}H_{23}N_7OS$, C 63.00, H 5.07, N 21.43 found C 62.78, H 5.31, N 21.278.

Biological evaluation

***In vitro* anti-proliferative activity against 60 cell line panel.** NCI *in vitro* cancer screening is a two-phase process that begins with the evaluation of all compounds against the 60 NCI cell line panel, which includes cell lines representing leukemia, NSCLC, CNS cancer, melanoma, prostate cancer, breast cancer, renal cancer, colon cancer, and ovarian cancer at a single point of 10 μM. The single dose output can be reported as a mean graph (ESI†).

FLT3 inhibitory assay. The *in vitro* enzyme inhibition assay for the synthesized compounds was carried out in Thermo Fisher Scientific, Life Technologies, USA (https://www.thermofischer.com/selectscreen). The assay was performed to evaluate the inhibitory activity of the compounds designed applying the Z′-LYTE biochemical assay employing a fluorescence-based, coupled-enzyme format based on the differential sensitivity of phosphorylate and non-phosphorylate peptides to the proteolytic cleavage.

Molecular docking. Molecular modeling was carried out using Molecular Operating Environment (MOE, 2015.10). Crystal structure of FLT3 kinase domain bound to the selective inhibitor was obtained from Protein Data Bank (https://www.rcsb.org/, PDB code: 4RT7, resolution of 3.20 Å). Water molecules and ligands which are not involved in the binding were removed. The partial charges were calculated automatically. Protein structure preparation protocol including 3D protonation & structure correction was used with its default MOE options to prepare the protein. Energy minimization was carried out then a validation step was performed for the docking protocol by re-docking of the co-crystallized inhibitor, and the obtained low RMSD value indicated the valid performance (RMSD = 1.46 Å).

The method used for docking was general docking. The scoring methodology was selected as GBVI/WSA dG for the refinement methodology. On the other hand, the scoring methodology was applied as London dG for the placement methodology, which was selected as a triangle matcher. The applied forcefield was Amber10:EHT. The prepared MDB file was inserted containing all newly synthesized compounds then docking calculations was performed automatically. Only one pose was selected for each compound and the selection was based on the binding scores, rmsd_refine values, and interaction modes (ESI†).

Molecular dynamics. At NPT ensemble, the FLT3 crystal structure (PDB ID: 4RT7) was subjected to molecular dynamics simulation. The OpenMM Setup utility was used to set up the simulation system. MD was carried out for 50 ns for four compounds resulting in total of four MD runs. RMSD, RMSF and radius of gyration was calculated out using ProDy python library (ESI†).

***In silico* predictive ADME study for targeted compounds.** Using the Accelrys Discovery Studio 2.5 program, computer-ADMET analysis was carried out. These studies are based on the molecule's chemical structure and include the measurement of certain parameters, including atomic log*P*98 (*A* log *P*98), 2D polar surface area (ADMET 2D PSA), aqueous solubility (AQ SOl), aqueous solubility level (AQ SOl LEV), blood–brain barrier value (BBB), blood–brain barrier level (BBB LEV), cytochrome P450 2D6 (CYP2D6), cytochrome P450 2D6 probability (CYP PROB), logarithmic value of plasma protein binding (PPB LOG), and logarithmic level of plasma protein binding (PPB LEV).

Conflicts of interest

There are no conflicts to declare.

Acknowledgements

The authors would like to thank Prof. Dr Reem K. Arafa, Professor of Biomedical Sciences, University of Science and Technology, Zewail City of Science and Technology, Giza, Egypt for the assistance in molecular docking study.

Notes and references

1 S. A. Rostom, Synthesis and *in vitro* antitumor evaluation of some indeno [1, 2-c] pyrazol (in) es substituted with sulfonamide, sulfonylurea (-thiourea) pharmacophores, and some derived thiazole ring systems, *Bioorg. Med. Chem.*, 2006, **14**(19), 6475–6485.

2 L. A. Torre, *et al.*, Global cancer statistics, 2012, *Ca-Cancer J. Clin.*, 2015, **65**(2), 87–108.

3 P. Blum-Jensen and T. Hunter, Oncogenic kinase signaling, *Nature*, 2001, **411**(3), 355–365.
4 N. N. Kabir and J. U. Kazi, Comparative analysis of human and bovine protein kinases reveals unique relationship and functional diversity, *Genet. Mol. Biol.*, 2011, **34**(4), 587–591.
5 J. A. Orgueira, D. A. Pérez, *et al.*, FLT3 inhibitors in the treatment of acute myeloid leukemia: current status and future perspectives, *Minerva Med.*, 2020, **111**(5), 427–444.
6 E. Weisberg, *et al.*, Inhibition of mutant FLT3 receptors in leukemia cells by the small molecule tyrosine kinase inhibitor PKC412, *Cancer Cell*, 2002, **1**(5), 433–443.
7 M. Levis, *et al.*, A FLT3-targeted tyrosine kinase inhibitor is cytotoxic to leukemia cells *in vitro* and *in vivo*, *Blood*, 2002, **99**(11), 3885–3891.
8 L. M. Kelly, *et al.*, CT53518, a novel selective FLT3 antagonist for the treatment of acute myelogenous leukemia (AML), *Cancer Cell*, 2002, **1**(5), 421–432.
9 D. E. L. de Menezes, *et al.*, CHIR-258: a potent inhibitor of FLT3 kinase in experimental tumor xenograft models of human acute myelogenous leukemia, *Clin. Cancer Res.*, 2005, **11**(14), 5281–5291.
10 A.-M. O'Farrell, *et al.*, *SU11248 is a novel FLT3 tyrosine kinase inhibitor with potent activity in vitro and in vivo*, *Blood*, 2003, **101**(9), 3597–3605.
11 J. M. Gozgit, *et al.*, Potent activity of ponatinib (AP24534) in models of FLT3-driven acute myeloid leukemia and other hematologic malignancies, *Mol. Cancer Ther.*, 2011, **10**(6), 1028–1035.
12 E. Lierman, *et al.*, The ability of sorafenib to inhibit oncogenic PDGFRβ and FLT3 mutants and overcome resistance to other small molecule inhibitors, *Haematologica*, 2007, **92**(1), 27–34.
13 P. Baxter, *et al.*, Plasma and cerebrospinal fluid pharmacokinetics of MP470 in non-human primates, *Cancer Chemother. Pharmacol.*, 2011, **67**(4), 809–812.
14 S. Scholl, *et al.*, Molecular Mechanisms of Resistance to FLT3 Inhibitors in Acute Myeloid Leukemia: Ongoing Challenges and Future Treatments, *Cells*, 2020, **9**(11), 2493.
15 L. Y. Lee, *et al.*, Preclinical studies of gilteritinib, a next-generation FLT3 inhibitor, *Blood*, 2017, **129**(2), 257–260.
16 P. P. Zarrinkar and et al, ., AC220 is a uniquely potent and selective inhibitor of FLT3 for the treatment of acute myeloid leukemia (AML), *Blood*, 2009, **114**(14), 2984–2992.
17 E. I. Zimmerman, *et al.*, Crenolanib is active against models of drug-resistant FLT3-ITD-positive acute myeloid leukemia, *Blood*, 2013, **122**(22), 3607–3615.
18 S. Bertoli, *et al.*, Outcome of Relapsed or Refractory FLT3-Mutated Acute Myeloid Leukemia before Second-Generation FLT3 Tyrosine Kinase Inhibitors: A Toulouse–Bordeaux DATAML Registry Study, *Cancers*, 2020, **12**(4), 773.
19 C. N. Khobragade, *et al.*, Synthesis and antimicrobial activity of novel pyrazolo [3, 4-d] pyrimidin derivatives, *Eur. J. Med. Chem.*, 2010, **45**(4), 1635–1638.
20 A. E. Rashad, *et al.*, Synthesis and antiviral evaluation of some new pyrazole and fused pyrazolopyrimidine derivatives, *Bioorg. Med. Chem.*, 2008, **16**(15), 7102–7106.
21 S. B. Yewale, *et al.*, Novel 3-substituted-1-aryl-5-phenyl-6-anilinopyrazolo [3, 4-d] pyrimidin-4-ones: docking, synthesis and pharmacological evaluation as a potential anti-inflammatory agents, *Bioorg. Med. Chem. Lett.*, 2012, **22**(21), 6616–6620.
22 M. Celano, *et al.*, Cytotoxic effects of a novel pyrazolopyrimidine derivative entrapped in liposomes in anaplastic thyroid cancer cells *in vitro* and in xenograft tumors *in vivo*, *Endocr.-Relat. Cancer*, 2008, **15**(2), 499–510.
23 J.-Y. Le Brazidec, *et al.*, Synthesis, SAR and biological evaluation of 1, 6-disubstituted-1*H*-pyrazolo [3, 4-d] pyrimidines as dual inhibitors of Aurora kinases and CDK1, *Bioorg. Med. Chem. Lett.*, 2012, **22**(5), 2070–2074.
24 A. Spreafico, *et al.*, Antiproliferative and proapoptotic activities of new pyrazolo [3, 4-d] pyrimidine derivative Src kinase inhibitors in human osteosarcoma cells, *FASEB J.*, 2008, **22**(5), 1560–1571.
25 F. Manetti, *et al.*, Structure-based optimization of pyrazolo [3, 4-d] pyrimidines as Abl inhibitors and antiproliferative agents toward human leukemia cell lines, *J. Med. Chem.*, 2008, **51**(5), 1252–1259.
26 N. S. Ismail, *et al.*, Pyrazolo [3, 4-d] pyrimidine based scaffold derivatives targeting kinases as anticancer agents, *Future J. Pharm. Sci.*, 2016, **2**(1), 20–30.
27 C. La Motta, *et al.*, Exploiting the pyrazolo [3, 4-d] pyrimidin-4-one ring system as a useful template to obtain potent adenosine deaminase inhibitors, *J. Med. Chem.*, 2009, **52**(6), 1681–1692.
28 A. A. Gaber, *et al.*, Pharmacophore-linked pyrazolo [3, 4-d] pyrimidines as EGFR-TK inhibitors: synthesis, anticancer evaluation, pharmacokinetics, and *in silico* mechanistic studies, *Arch. Pharm.*, 2021, e2100258.
29 L.-L. Yang, *et al.*, Structure–activity relationship studies of pyrazolo [3, 4-d] pyrimidine derivatives leading to the discovery of a novel multikinase inhibitor that potently inhibits FLT3 and VEGFR2 and evaluation of its activity against acute myeloid leukemia *in vitro* and *in vivo*, *J. Med. Chem.*, 2013, **56**(4), 1641–1655.
30 G.-B. Li, *et al.*, Drug Discovery against Psoriasis: Identification of a New Potent FMS-like Tyrosine Kinase 3 (FLT3) Inhibitor, 1-(4-((1 H-Pyrazolo [3, 4-d] pyrimidin-4-yl) oxy)-3-fluorophenyl)-3-(5-(tert-butyl) isoxazol-3-yl) urea, That Showed Potent Activity in a Psoriatic Animal Model, *J. Med. Chem.*, 2016, **59**(18), 8293–8305.
31 A. Agrebi, *et al.*, Synthesis and biological evaluation of new pyrazolo [3, 4-d] pyrimidine derivatives, *Mediterr. J. Chem.*, 2014, **3**(2), 864–876.
32 M. M. Kandeel, *et al.*, Design, synthesis, and antitumor evaluation of novel pyrazolo [3, 4-d] pyrimidine derivatives, *Sci. Pharm.*, 2012, **80**(3), 531–546.
33 K. Matsuno, *et al.*, Nitrogenous heterocyclic compounds, *European Patent*, 1999, EP1067123.
34 M. G. Salem, *et al.*, Synthesis, molecular modeling, selective aldose reductase inhibition and hypoglycemic activity of novel meglitinides, *Bioorg. Chem.*, 2021, **111**, 104909.

35 H. D. Souza, *et al.*, Synthesis, *in silico* study and antimicrobial evaluation of new selenoglycolicamides, *J. Braz. Chem. Soc.*, 2019, **30**, 188–197.
36 R. Mishra, *et al.*, Synthesis and Anticonvulsant Activity of Some Novel 2-Methyl Imidazole Derivatives, *Lett. Drug Des. Discovery*, 2012, **9**(4), 402–408.
37 A. M. Qandil and L. I. Fakhouri, a-Anilinoketones, esters and amides: a chemical study, *Pharmaceuticals*, 2012, **5**(6), 591–612.
38 K. H. Oudah, *et al.*, Design, synthesis and molecular docking of novel pyrazolo [1, 5-a][1, 3, 5] triazine derivatives as CDK2 inhibitors, *Bioorg. Chem.*, 2019, **92**, 103239.
39 D. R. Parmar, *et al.*, Discovery of new anticancer thiourea-azetidine hybrids: design, synthesis, *in vitro* antiproliferative, SAR, *in silico* molecular docking against VEGFR-2, ADMET, toxicity, and DFT studies, *Bioorg. Chem.*, 2021, **115**, 105206.